Investigation of the Effect of Changes in Lipid Bilayer Properties on the Activity of the Bacterial Cell Division Regulator Protein MinD

Saud Ayed

Thesis submitted to the
Faculty of graduate and postdoctoral studies
University of Ottawa

In partial fulfillment of the requirements for the degree of
Masters of science in biochemistry

uOttawa

L'Université canadienne
Canada's university

Department of Biochemistry, Microbiology and Immunology
Faculty of Medicine

Abstract

Bacterial cell division requires formation of the cytokinetic cell division septum at the mid-cell position, a process that is determined by three Min proteins; MinC, MinD and MinE. Regulation of cell division by Min proteins occurs via a multi-step process involving interactions between various Min proteins, as well as the membrane. In this cycle, ATP-bound MinD binds to the membrane surface where it can recruit MinC to inhibit formation of the cell division septum. MinE binding to this complex displaces MinC and stimulates ATP hydrolysis, leading to the dissociation of MinD from the membrane. These interactions give rise to a dynamic pattern of Min protein localization that appears to involve a polymeric state that is designed to create a zone that is permissive to cell division at the mid-point of the cell. The interaction between MinD and the membrane is a critical aspect of this cycle, yet the role of the lipid bilayer in MinD activation, localization and polymerization is not well understood. To probe the role of membrane charge and fluidity on MinD activation and polymerization, we developed a kinetic assay of MinE-stimulated MinD ATPase activity. We found that membrane charge is essential for MinD activation and that differences in membrane fluidity give rise to changes in its activity. Moreover, a burst phase was also observed during the first few minutes of reaction, but only on the most fluid anionic lipid tested. To help determine if the observed membrane-dependent changes in MinD activity are linked to any changes in MinD polymer structure, we have begun to develop a method to identify surface exposed regions of MinD through a combination of covalent labeling and mass spectrometry. Optimization of various steps for the assay has been done, and the assay can be applied to the future characterization of MinD polymer structure. Results from this assay, in combination with those from the kinetic measurements described here, will help to improve understanding about how membrane properties modulate MinD ATPase activity, and how this can influence the Min protein oscillation that is required to ensure normal bacterial cell division.

Table of Contents

List of Figures

List of tables

List of abbreviations

CL	Cardiolipin
DOPG	1,2-di-(9Z-octadecenoyl)-sn-glycero-3-phospho-(1'-rac-glycerol)
DOPC	1,2-dioleoyl-sn-glycero-3-phosphocholine
EI	Electrospray Ionization
Ec	*Escherichia coli*
FRET	Förster resonance energy transfer
Fenton solution	Ferrous ammonium persulfate
h	Hill coefficient
HDX	Hydrogen/deuterium exchange
IPTG	Isopropyl β-D-1-thiogalactopyranoside
k_{cat}	Catalytic constant
$K_{0.5}$	Concentration of ligand (L) required to reach half-maximal activity
LC	Liquid chromatography
LUV	Large unilamellar vesicles
MS	Mass spectrometry
MALDI	Matrix-assisted laser desorption/ionization
NMR	Nuclear magnetic resonance
Ng	*Neisseria gonorrhoeae*
Pi	Inorganic phosphate
PG	Phosphoglycerol
POPG	1-palmitoyl-2-oleoyl-sn-glycero-3-phospho-(1'-rac-glycerol)
PC	Phosphocholine
PE	Phosphatidylethanolamine
RDM	Reaction diffusion model
RCD	*E. coli* GlpG rhomboid protein
SUV	Sonicated unilamellar vesicles
TIRF	Total internal reflection fluorescence
T_m	Melting temperature
V_{max}	Maximal enzymatic rate
θ	Fraction of available occupied ligand (MinE)-binding sites in enzyme (MinD)

Acknowledgement

Dr. Natalie Goto for her support and for allowing me to conduct research on a wonderful topic. I have acquired so many skills under her vision. I appreciate having her as supervisor.

My committee members; Dr. John Pezacki and Dr. Mary Hefford

Dr. Houman Ghasriani for his help especially for clarifying the physics behind the instruments.

Dr. Jeff Smith for his help with LC-MS/MS.

Fatima Hafizi for teaching me FPLC and MinD ATPase assay.

Laura McLeod for discussing ideas on Min system.

Dr. Allison Sherratt for her help with DNA purifications.

Tabussom Qureshi for your great moments.

Dr. Tom Moon's lab namely; Shahram Eisa-Beygi and Aziz Alhabsi for allowing me to use spectrophotometer.

Dr. Maxim Berezovski's lab namely; Gleb Mironov for conducting MSMS experiments.

Dr. Robert Ben's lab; namely, Dr. Mathieu Leclère for introducing MALDI to me.

Dr. Chris Boddy's lab (Luis Villegas) for his help with MALDI.

Christian Prud'homme (Biochemistry Head Technologist) for HPLC analysis.

Finally, my parents for encouraging me to pursue higher education.

Chapter 1: Introduction

1.1 Min proteins in bacterial cell division

The propagation of bacterial populations relies on the ability of bacterial cells to undergo the finely controlled process of binary fission into two equal-sized daughter cells. This occurs through the formation of the cytokinetic cell division septum at the mid-cell position. An important control mechanism utilized by gram negative bacteria to ensure proper placement of this septum is provided by the Min system, comprised of three proteins encoded by the *minB* operon; MinC, MinD and MinE (1). Defects in any one of these proteins results in either a filamentous phenotype and/or minicells, non-productive products of cell division that contain none of the chromosomal material required for subsequent rounds of cell division (2-4). Min proteins are responsible for preventing cell division at polar sites, helping to restrict cell division to the midcell position.

The importance of the Min system for the promotion of symmetric bacterial cell division makes it a potential target for the development new antimicrobial compounds, especially since MinE does not have a homologue in humans. Consequently, if we can better understand how the Min system functions then this will facilitate the development of a strategy for its inhibition, a goal of particular interest in the case of pathogenic species. Min proteins from one such pathogen are the focus of the work in this thesis, namely *Neisseria gonorrhoeae.* This species is responsible for the sexually transmitted disease called gonorrhea that is widespread in Africa, but increasing in prevalence in North America (5). Of particular concern is the fact that poor treatment of *N. gonorrhoeae* infections has given rise to the development of resistant strains. For instance, a new multidrug resistant strain of *N. gonorrhoeae* has appeared in Ontario in recent years (6, 7). This decrease in the efficacy of antibiotics against *N. gonorrhoeae* has been correlated with antibiotic misuse and disposal (8), necessitating the development of new antimicrobial agents.

Although our lab has been interested in the Min proteins from *N. gonorrhoeae* ($MinD_{Ng}$, $MinE_{Ng}$), the majority of the knowledge that has been developed on Min proteins to date has come from the *E. coli* proteins (9). However many of these studies provide strong evidence that the *N. gonorrhoeae* (Ng) proteins work in the same way as the *E. coli* homologues. For example, $MinD_{Ng}$ or $MinE_{Ng}$ can replace the *E. coli* proteins since they share significant structural and functional similarities (10). There is a high degree of sequence similarity between Min proteins from the two organisms, with 42% and 75% sequence identity for MinE and MinD, respectively (Fig. 1.1). This high level of sequence homology, and functional complementarity of the Ec and Ng proteins suggest that their structures will also be highly similar. Ultimately we would like to gain a better understanding of how the Min system works at the molecular level, a goal that I have been working towards through my study of the Min proteins from Ng.

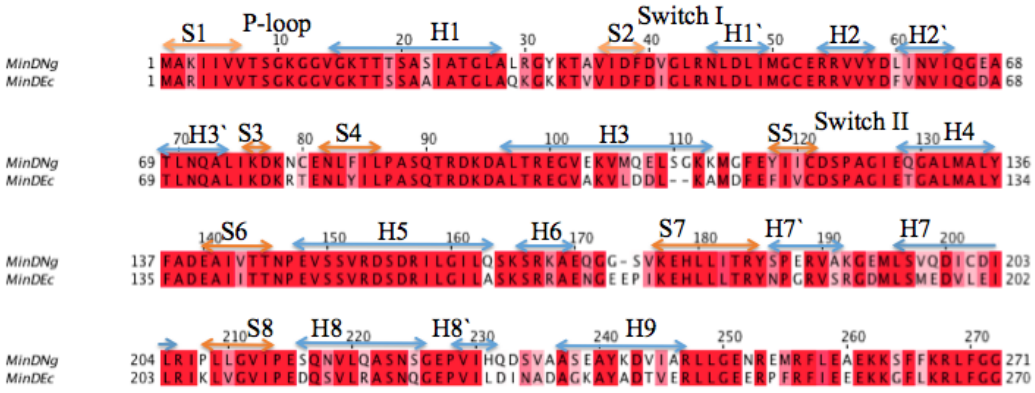

Figure 1.1: $MinD_{Ng}$ and $MinD_{Ec}$ amino acid sequence alignment. *Sequence alignment was preformed with ClustalW2 (11) and sequence coloring of the alignment was done using Jalview (12). Red regions correspond to identical residues, and light red regions show homologous residues. Sequence identity is 75%. Secondary structure elements from the E. coli structure are shown above the sequence as blue arrows for α helical regions and orange arrows for β strands. Secondary structures were labeled according to (13).*

1.2 Interactions between Min proteins

Min proteins act to prevent cell division at the cell poles through interactions with FtsZ, a protein that nucleates formation of the cell division septum (3, 14-16). In this process FtsZ is recruited to the cell membrane by binding to ZipA and FtsA proteins, polymerizing to form a structure called the Z ring (17). Interactions between MinC and FtsZ inhibit FtsZ polymerization in a site-specific manner, with Z-ring formation only being allowed at the mid-cell position (14). Loss of Min proteins or overexpression of FtsZ removes this restriction on Z-ring placement, giving rise to cell division at both polar and mid-cell positions of the cell (2-4, 18). Coordinated interactions between Min proteins function together to prevent the energetically expensive process of cell division from occurring at the non-productive polar sites.

A number of biochemical studies on the Min proteins have provided important details regarding their interactions, and how they might restrict cell division to the midcell location. This begins with interactions between MinD and ATP, with size exclusion chromatography studies showing that ADP-bound MinD is monomeric, but becomes a dimer upon nucleotide exchange with ATP (19). In this ATP-bound dimeric state, MinD is able to bind to the membrane by a ~15-residue C-terminal sequence called the membrane targeting sequence (MTS) (19-22). *In vitro* tryptophan fluorescence studies demonstrated that dimerization causes MinD to undergo a conformational change that appears to expose the MTS for membrane interactions (23). *In vitro* sedimentation assays of lipid vesicle-bound MinD showed that the complex was resistant to high salt concentrations suggesting that the interaction was at least partially mediated by hydrophobic residues partitioning into the hydrophobic phase of the bilayer (21).

As demonstrated in yeast two hybrid (15, 21) and vesicle sedimentation studies (24, 25), when MinD is in the membrane-bound state it can bind to MinC. The membrane-bound MinCD complex is known as the inhibitory complex (16) since it inhibits cell septum formation by interfering with the polymerization of FtsZ (26), a critical step for the nucleation of the cell division septum (14). Inhibition of FtsZ appears

to occur through direct interactions between MinC and FtsZ, with *in vitro* sedimentation studies showing that the amount of pelleted FtsZ polymers could be reduced by increasing concentrations of MinC (15, 27). In addition, *in vitro* FRET experiments also showed that MinC interacts with monomeric FtsZ (27). Meanwhile the rate of FtsZ GTPase activity is not altered by MinC (14), consistent with the idea that MinC interactions with monomeric FtsZ can enhance the extent of FtsZ disassociation from its polymer rather than destabilizing the polymer through an increased rate of GTP hydrolysis.

A number of biochemical studies have shown that inhibition of cell division by the membrane-bound MinCD complex can be relieved by direct interactions between MinE and MinD. Specifically, vesicle sedimentation studies showed that MinE localized to the pellet fraction, but only when MinD and ATP were also present (25). Yeast three-hybrid experiments also showed that the MinCD complex could be disrupted by MinE (16, 28) suggesting that MinE competes with MinC for an overlapping binding site on MinD. However, the interaction with MinE may be of higher affinity since vesicle sedimentation studies show that MinE could displace MinC from MinD, while MinC was not able to displace MinE (29).

Another event that is triggered by MinE binding to MinD is stimulation of the MinD ATPase activity. *In vitro* assays of ATPase activity have shown that MinE stimulates MinD-catalyzed ATP hydrolysis rates by a factor of approximately 10-fold (30-32). Vesicle sedimentation studies with MinD also showed that MinE destabilizes the MinD-membrane interaction resulting in dissociation of MinD from membrane (25). Therefore ATP hydrolysis generates the monomeric, ADP-bound form of MinD in the cytoplasm where it can once again undergo nucleotide exchange, membrane localization and MinC binding to restore the inhibitory MinCD complex (10, 26). The resulting cycle of Min protein interactions can be summarized in a schematic model (Fig. 1.2) showing ATP-dependent generation of the membrane-bound MinCD complex that is disrupted by interactions with MinE, stimulating ATP hydrolysis.

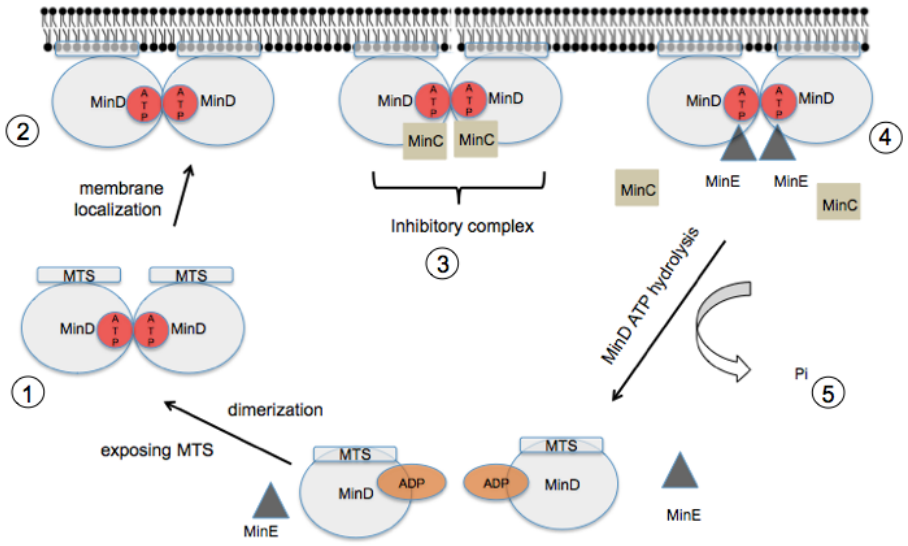

Figure 1.2: The Min protein interaction cycle. *1) MinD forms a dimer when bound to ATP followed by 2) localization to cell membrane. 3) MinD recruits MinC to the membrane, forming a complex that inhibits FtsZ polymerization. 4) MinE binds to MinD on a site that overlaps with the MinC binding site, resulting in displacement of MinC. 5) MinE stimulates MinD ATP hydrolysis, leading to dissociation from the cell membrane and generation of monomeric ADP-bound MinD so that the cycle can start again.*

1.3 MinD structure

High resolution structural information is now available for all of the proteins that participate in the Min cycle (13, 31, 33, 34), including MinD, the main focus of my thesis. This includes an x-ray structure of MinD from a hydrolysis-deficient mutant (D40N) of the *E. coli* protein ($MinD_{Ec}$) in a dimeric complex bound to ATP (35). As shown in this structure, each MinD subunit consists of a central β sheet composed of 8 parallel strands as well as 11 peripheral α helices (35, 36).

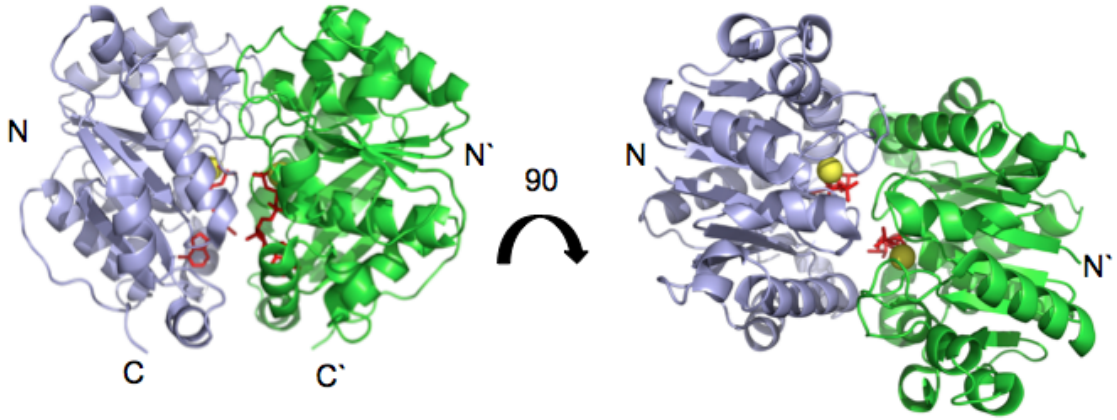

Figure 1.3: Crystal structure of the $MinD_{Ec}$ dimer in the presence of ATP and Mg^{2+}. *Ribbon diagram of two views of the MinD dimer formed in the presence of ATP (red) and Mg^{2+} (yellow) with each subunit shown in a different color (green or blue). The structure shown is the ATP-bound hydrolysis-deficient mutant of E. coli MinD D40N (PDB:3Q9L) (35). Note that ten residues from the C-terminus, responsible for membrane binding, is also not included in this structure, having been removed to facilitate crystallization.*

MinD belongs to Par-family of ATPases which are characterized by a distinctive deviant Walker A motif that promotes direct contact with phosphate groups of ATP (13, 37). The ATP binding site is partially formed by a conserved sequence located between β1 and α1 called the P-loop, responsible for binding to ATP phosphate groups. As shown in Figure 1.4, P-loop residues G13, G15 and K16 make hydrogen bonds with β and γ phosphoryl oxygen atoms whereas, T17 and T18 hydrogen bonds to the α phosphate (33). Two other loops called switch I and switch II contain residues that interact with the γ phosphate group (13). In addition, D118 and C119 in switch II bind to water molecules that coordinate with the bound Mg^{2+} ion, an interaction that is likely to be important for catalysis (33).

The structure of this MinD dimer also highlighted the importance of ATP-binding in dimer formation, with each bound molecule of ATP being buried in the dimeric interface. A number of specific interactions were identified between residues from one subunit and the ATP located in the nucleotide-binding cleft of the other subunit (35). As shown in Figure 1.4, these include hydrogen bonding interactions involving P-loop residues K11 and G12 to phosphate groups of the ATP bound to the other subunit. The

importance of these intermolecular interactions between ATP and MinD across the dimeric interface has been confirmed by experiments with mutants of these residues (35, 38). For example, size exclusion chromatography of the *E. coli* MinD K11A mutant showed that it could not dimerize in presence of ATP (38).

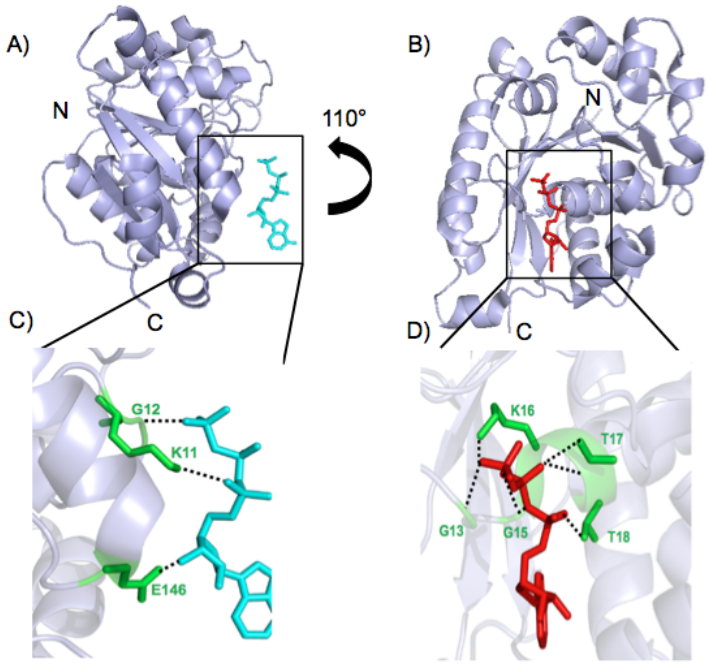

Figure 1.4: ATP binding site of MinD$_{Ec}$. *A) and B) Two views of a single subunit from the structure shown in Figure 1.3 with ATP from the other subunit shown in cyan, and the same subunit in red. C) Expanded view of the ATP-binding pocket highlighting MinD residues that interact with ATP bound to the other MinD subunit, or D), the same subunit, with dashed lines denoting hydrogen bonds.*

In addition to the MinD dimer structure, a structure of this same MinD mutant in complex with the MinD-binding domain of MinE (residues 13 – 30) has recently been determined (39). This structure shows that MinE binds in a helical conformation to the MinD dimer interface, with interactions involving residues from both subunits of MinD to a single MinE helix (Figure 1.5). The importance of these interactions was confirmed by bacterial two hybrid analysis showing that mutation of residues L48, E53, G191, D198, S221 or N222 in MinD reduced binding to MinE (35, 39). This is consistent with a number of earlier studies that identified these residues as being important for MinE binding activity (35, 38). In addition, results from bacterial two-hybrid studies of the

MinD-MinC interaction, when mapped onto the MinD dimer structure, show some of the residues important for this interaction also bind to MinE (35, 38) (Fig. 1.5 B) supporting the idea of overlapping binding sites on MinD for these two proteins.

Although these structures have provided an unprecedented level of detail to the MinD-MinE interaction, it is still not known how MinE binding stimulates hydrolysis of ATP. However, one of the components that is required for this stimulation to occur is the lipid membrane, since MinD appears to be completely inactive in absence of lipids (30). The structure of the MinD-MinE complex provides some suggestion as to how it might sit on the membrane, based on the position of the C-termini of the truncated MinD. Although the membrane-targeting sequences were not included in the samples that gave rise to these structures, it appears that they would lie on the membrane, in such a way that places the MinE-binding site in close proximity to the membrane surface (Fig. 1.5A). Nonetheless, it is not yet known if this view of the membrane-bound state is accurate, and what additional changes in structure might occur to promote ATP hydrolysis. More importantly these structures alone do not explain how the Min proteins use this cycle of interactions to only inhibit cell division at the polar site of the cell. In order to gain better insight into this mechanism it has been necessary to use fluorescence microscopy to examine the behavior of Min proteins *in vivo*, and in reconstituted systems *in vitro*.

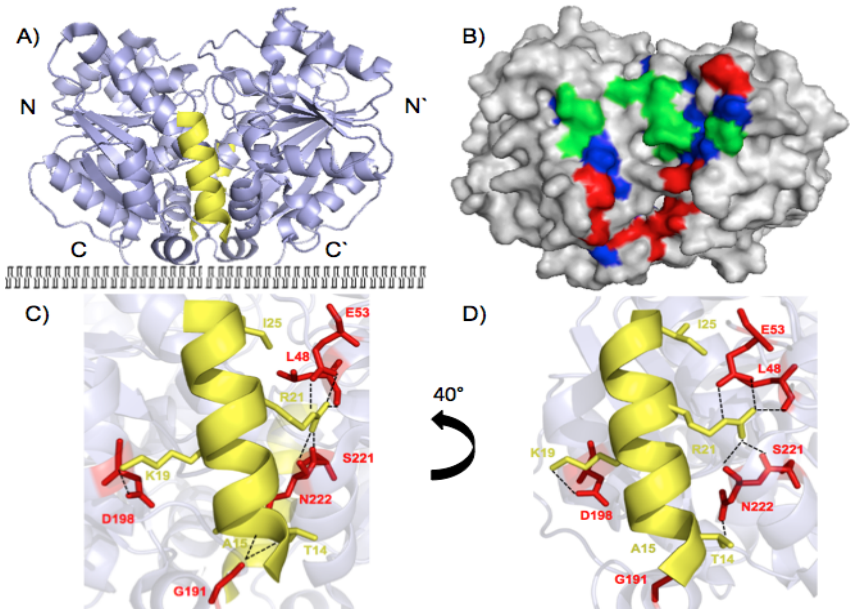

Figure 1.5: Structure of the MinD$_{Ec}$ complex with MinE residues 12-31. *A) Ribbon diagram view of the MinDEc dimer structure (light blue) in the same orientation shown in Figure 1.3, in complex with MinE$_{Ng}$ 12-31 (yellow) (PDB ID: 3R9I). A schematic representation of the putative location of the lipid bilayer, as deduced from the location of the C-termini that would be immediately adjacent to the membrane-targeting helix in the full-length protein. B) Surface representation of the MinD dimer structure (PDB:3Q9L) with residues involved in MinE binding highlighted in red, residues which when mutated disrupt binding to MinC in green, and residues thought to comprise overlapping regions of the MinE and MinC binding sites in blue. C and D) Expanded view of the MinE interaction surface on the MinD structure, with hydrogen bonding interactions indicated by dashed lines.*

1.4 Macromolecular organization and oscillation cycle of Min proteins

At the cellular level the cycle of Min interactions gives rise to the formation of dynamic subcellular complexes at the bacterial inner membrane (40). As shown in microscopy experiments with fluorescent protein-tagged Min proteins, MinD concentrates at the membrane on one side of the cell, forming a spiral subcellular structure around the circumference of the cell that extends from the cell pole towards the midcell (40). MinC colocalizes with this superstructure to form the inhibitory complex, although MinC itself is not required for this structure to form. Instead the superstructure seems to reflect an inherent tendency for MinD to polymerize on the cell membrane, as revealed by *in vitro* electron microscopy studies. Published images suggest that MinD

forms a polymeric superstructure that is assembled from filamentous bundles of MinD polymer when incubated with ATP and phospholipids (32, 41).

The polymer formed by MinD is not static, but has growth and decay phases that appear to be modulated by MinE (schematically outlined in Figure 1.6). As the subcellular coil structure formed by MinD extends toward the midcell, MinE forms an annular structure along this coil that has been called the E-ring (42). However, colocalization studies show that MinE also appears throughout the Min polymer, albeit at lower concentrations than seen at the edge of the polymer. Meanwhile, appearance of the E-ring coincides with dissociation of the MinD superstructure at the leading edge, with MinE remaining associated with this zone as it retracts toward the cell pole. At the same time, a new subcellular MinD superstructure begins to form at the opposite pole, and continues to grow towards the midpoint of the cell, being capped with a new E-ring structure when it reaches this point. The total time it takes for one cycle of growth and decay of these subcellular Min structures is approximately 30 to 40 seconds (20, 26). The net result of this dynamic formation and decay of the Min protein polymers is that the time-averaged concentration of MinE will remain highest at mid-cell, creating a zone that is permissive to formation of the cytokinetic cell division septum. Meanwhile, a high time-averaged concentration of the MinCD complex at the poles ensures that FtsZ polymer formation is inhibited at these sites, preventing minicell formation.

In vitro studies provide additional evidence that MinE directs the dissociation of the MinD polymer, with electron microscopy of MinD polymers showing their dissociation upon addition of MinE (41). Moreover, conditions giving rise to these MinD polymeric structures *in vitro* also show dynamic light scattering, the magnitude of which decreases over time after the addition of MinE (41). Based on these results it has been proposed that liberation of MinD from the membrane by MinE-stimulated MinD ATP hydrolysis generates cytoplasmic MinD that can then diffuse to the other cell pole to establish new polar zone. Similarly, once the E-ring completes the dissociation of the MinD polymer, free MinE molecules can diffuse through the cell to construct a new E

ring on the newly formed MinD subcellular structure extending from the opposite pole (43, 44).

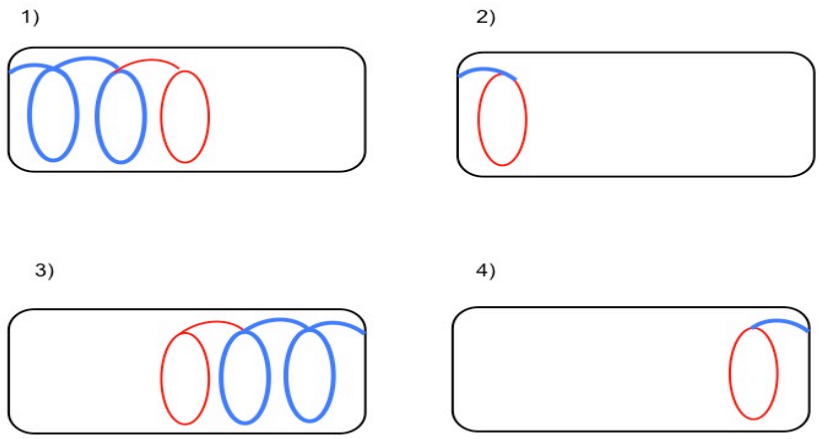

Figure 1.6: Schematic diagram of the pole to pole oscillation cycle of Min proteins. *A zone with a high concentration of the MinCD complex (solid blue) forms at the membrane at one side of the cell and MinE (solid red) localizes to the leading edge of this zone to form a subcellular annulus called the E-ring (1). The E-ring stimulates the dissociation of MinD from the membrane, following the edge of the MinCD zone as it retracts back toward the pole (2). Liberation of MinD from the membrane allows it to diffuse through the cell and establish a new MinCD zone at the other cell pole (3). Meanwhile complete dissociation of the MinCD zone at the original pole is accompanied by dissociation of the E ring, allowing MinE to be released to the cytoplasm to form a new E-ring at the mid-cell (4).*

1.5 Dynamic Pattern Formation by Min Proteins on Planar Lipid Bilayers

One of the most vivid demonstrations of dynamic pattern formation by the Min proteins was provided by the study of florescent-labeled MinD and MinE on a planar lipid bilayer. Upon addition of ATP to this system, ordered dynamic mesostructures become apparent, with MinD forming concentrated ridges of protein that move across the bilayer surface, capped by a more concentrated zone of MinE at the trailing end (43). In this system the velocity of the MinD surface wave is proportional to the molar ratio of MinE to MinD, suggesting that MinE destabilizes the MinD polymer by stimulating MinD ATP hydrolysis (43).

In an attempt determine the mechanism of Min protein pattern formation in this planar bilayer study, an *in silico* model was proposed (43) utilizing the Turing or reaction diffusion model (RDM) (45, 46). The general idea behind this model is that a homogeneous mixture of two reacting species with different diffusion properties can give rise to small inhomogeneities in concentration that can become amplified to form large-scale patterns (45). This can be simulated with a series of nonlinear differential equations that describe the rate of concentration change for each component in the system (i.e. MinE and MinD). In this model, the interaction between MinD and MinE on the membrane surface stimulates ATP hydrolysis and dissociation, increasing the local concentration of these proteins in the cytoplasm. This generates local inhomogeneities in cytoplasmic concentrations of MinE and MinD that can affect the tendency of these proteins to interact with the membrane and/or the Min polymer, and hence their diffusion though the cytoplasm. These inhomogeneities tend to become amplified and then coalesce into a pattern that resembles the oscillation of Min proteins that is seen *in vivo*. However, RDM models require that estimated values be used for a large number of parameters; e.g. rates of membrane binding, ATP hydrolysis, nucleotide exchange, and diffusion of cytoplasmic and membrane-bound forms. While reasonable estimates have generally been used, the ability to reproduce oscillation depends strongly on the values that are chosen. Therefore, the ability of RDM-based models to reproduce Min protein oscillation and surface waves in silco cannot be taken as conclusive evidence that this is the mechanism that is actually being used in Min protein oscillation.

In order to refine the models used to simulate the Min surface waves, additional data on the rates of Min protein diffusion and membrane residency times were obtained through more quantitative studies using total internal reflection fluorescence (TIRF) microscopy of fluorescent-labeled Min proteins on planar bilayers (44). In this system it was found that the concentration of MinD accumulates at a relatively steady rate before plateauing around the mid-point of the wave (Fig 1.7). At the same time the density of MinE also increases in a linear fashion, although at a slower rate than that of MinD. The accumulation of MinE does not plateau with MinD, however, but continues to rise beyond the MinD plateau until the ratio of MinE to MinD is slightly greater than one. At

this point the membrane-bound concentration of both MinE and MinD drop abruptly, rapidly coming off the membrane to bring the fluorescence back to initial levels before the cycle starts again.

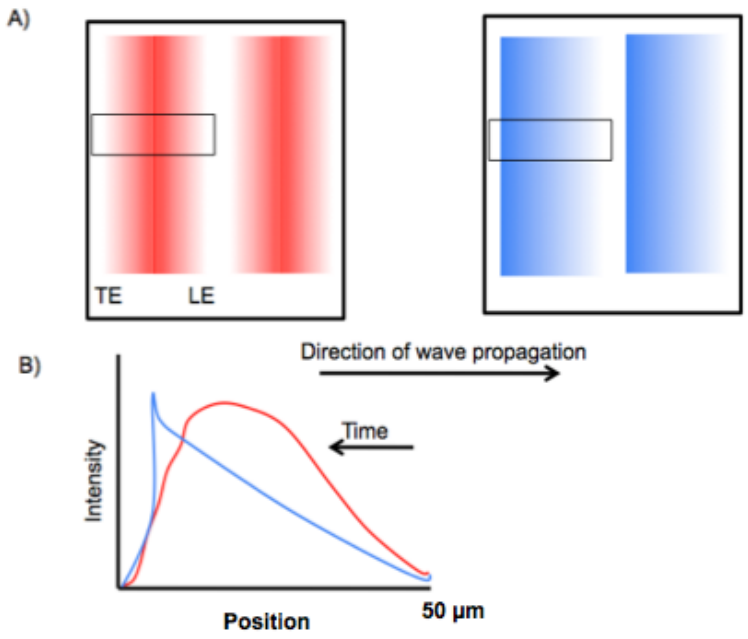

Figure 1.7: Schematic diagram of wave propagation dynamics of MinD and MinE proteins on supported lipid surface obtained by TIRF microscopy (44). *MinD (red) and MinE (blue) form planar waves that propagate across the bilayer surface A). MinD density is highest proximately at mid position towards trailing edge (TE) whereas, MinE density is highest at the TE and lowest at leading edge (LE). B) A cross section of the MinD/E wave shown in A).*

Forster resonance energy transfer (FRET) fluorescence microscopy was also done in this study, using donor and acceptor labeled MinE. The efficiency of energy transfer across the wave was found to be constant, suggesting that the accumulation of MinE at the trailing edge of the wave could not be attributed to cooperative effects in the MinE interaction with MinD. Single molecule TIRF of samples containing a small fraction of fluorescent-labeled protein also allowed diffusion rates of wave-associated Min proteins to be measured, with MinE diffusing at a three times faster rate than that for MinD. Residence times on the membrane were also slightly longer for MinE compared to MinD, suggesting that when MinE dissociates from MinD, it may rapidly reassociate with the polymer. These findings suggested that MinE accumulation at the trailing edge of MinD

wave is a result of MinE wave propagation by rapid rebinding to the polymer. This idea was supported by photobleaching experiments showing that when MinE in the central region of a propagating wave was photobleached, the intensity of MinE fluorescence at the trailing edge was not recovered as the wave passed through the photobleached area. This suggests that photobleached MinE did not dissociate from the membrane and get replaced with photoactive MinE, but rather remained within the wave until the wave had reached its peak and then dissipated from the membrane surface.

Taken altogether, the results from this landmark study have given rise to a new model of Min protein wave generation where MinD and MinE accumulate on the membrane and MinE can remain bound to the polymer. In this model, MinE binds weakly to the MinD polymer, undergoing a rapid cycle of binding and release without any requirement for ATP hydrolysis. This weak association allows MinE to accumulate along the polymer to form a concentrated zone at the trailing edge of MinD wave. When the binding sites at the end of the MinD polymer become saturated, MinD-catalyzed ATP hydrolysis is proposed to occur, resulting in MinD detachment from membrane.

While this model represents a significant advance in our understanding of how Min proteins form the mesoscale wave structures on planar lipid bilayers, a number of questions remain regarding how this relates to oscillation *in vivo*. In particular, it is not known why the MinD polymer undergoes a growth phase, or why the decay phase always starts at the mid-point of the cell. One potential factor that was not considered in these studies is the influence of various physical characteristics of the lipid bilayer on Min protein pattern formation, a question that I was interested in exploring in my thesis.

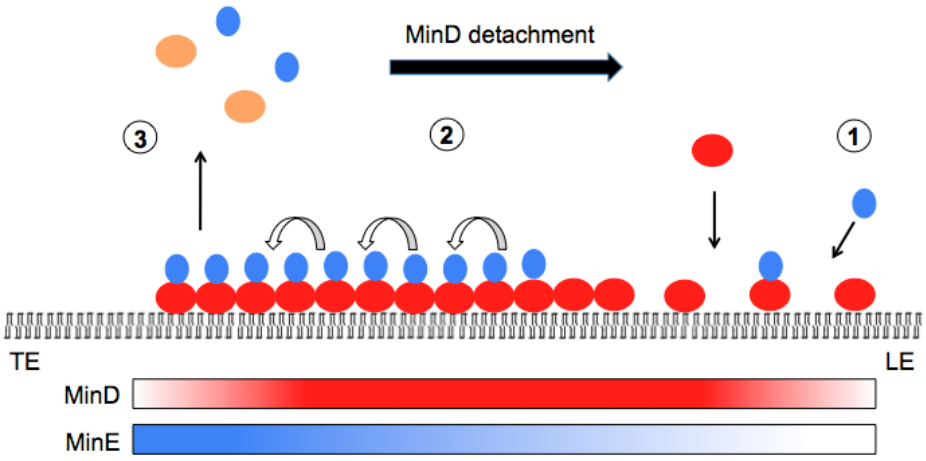

Figure 1.8: Schematic illustration of the rapid rebinding model of Min wave propagation proposed by Loose et al (44). *1) MinD attaches to membrane at the leading edge (LE). 2) MinE undergoes rapid binding and dissociation events that are not necessarily coupled with ATP hydrolysis. As a result of rapid rebinding, MinE accumulates at the trailing edge (TE) of the MinD polymer. 3) Once the binding sites of MinD polymer at the TE became saturated with bound MinE, MinE stimulates MinD ATP hydrolysis leading to detachment from membrane where monomeric MinD (orange) is free to diffuse to the other cell pole.*

1.6 MinD-membrane interaction

As described in previous sections, the MinD-membrane interaction plays a crucial role in the regulation of bacterial cell division by the Min system, and is required for MinD-catalyzed ATP hydrolysis to occur. Given the importance of this interaction we are interested in understanding the effect of the lipid environment on MinD activity, polymer formation and oscillation *in vivo*. Some progress toward this goal has been made in previous studies using *in vitro* sedimentation of lipid-bound MinD on vesicles comprised of lipids having a range of charge and fluidity properties (47). Results from this study showed that lipids with anionic headgroups gave rise to a 9-fold stronger interaction with MinD over that with neutral lipids. Similarly, lipids with lower phase transition temperatures also showed increased MinD-binding affinity (48). Moreover, when PG/PC lipid mixtures were used that gave rise to microdomains of fluid-phase anionic lipid embedded in a largely gel-phase bilayer, the affinity of MinD was significantly enhanced relative to fully fluid PG/PC mixtures. These results raise the possibility that the phase

and charge properties of the lipid bilayer may play a role in determining the morphology and dynamics of MinD subcellular structures.

The effect of membrane lipid compositions on Min protein oscillation has also been studied *in vivo*. For example, when PE lipid synthase was knocked out in *E. coli*, the resulting cells were filamentous, and normal Min oscillation was lost, with MinD instead moving as compact spots or clusters on the membrane in zigzag fashion (47). In contrast, PG-free *E. coli* gives rise to MinD that is localized mainly to the cell poles and at mid-cell. Coincidently, these are the regions of the cell where CL concentrations are highest, with CL-microdomains forming at the mid-cell of dividing cells that subsequently become the poles of the daughter cells (49, 50). This localization pattern reflects the lipid-binding properties observed *in vitro*, with CL being the only negatively charged lipid available in this knockout strain.

There is also significant evidence that MinD binding to lipid membranes alters the physical properties of the bilayer. Specifically, in studies with fluorescent probes of bilayer order using lipid vesicles comprised of synthetic lipids, or native inverted cytoplasmic membranes from *E. coli*, significant increases in membrane viscosity and order upon MinD binding were observed (48, 51). Moreover, mobility changes in pyrene-labeled PG induced by MinD binding suggested that MinD could induce some segregation of acidic lipids from a mixture of acidic and zwitterioinic lipids. Meanwhile, larger-scale structural changes in the membrane can also be imposed by interactions with MinD, as shown by electron microscopy of lipid vesicle bound MinD. When relatively high protein:lipid ratios are used, large unilamellar vesicles formed from *E. coli* lipid extracts can be deformed into tubules coated by MinD in an ATP-dependent process (32, 41, 52). Although deformation of the inner membrane does not occur *in vivo* since the concentration of MinD is not as high as the concentrations used in these studies, these structures may reflect more localized structural effects that could arise from higher concentrations of MinD bound to the pole.

Given the interplay between MinD-membrane interactions and the physical properties of the lipid bilayer, it is likely that the properties of the bilayer can also affect

MinD polymer formation. This is supported by the *in vivo* experiments with PE or PG knockouts of *E. coli* that show altered morphology of MinD subcellular structures (49, 50, 53). Similar results have also been observed on planar lipid bilayers with fluorescent-labeled MinD and MinE on membranes comprised of mixtures of synthetic lipids. This allowed the effects of different lipid properties on the structure and the dynamics of mesoscale Min structures formed (54). When bilayers were comprised of mono-unsaturated acyl chains with a headgroup composition mimicking that of *E. coli* lipid membranes was used, propagating waves similar to those observed on membranes comprised of *E. coli* lipids were observed when the experiment was performed at room temperature. However, when the experiment was performed at a slightly higher temperature (25°C), promoting a more fluid phase of the supported bilayer, dynamic 'amoeba' shaped structures were observed with a central island of MinD lined by a concentrated zone of MinE. The MinD center of smaller amoeba tends to shrink, with MinE disappearing from the structure when the MinD zone has disappeared, while large amoebas grow and are divided by the MinE zones into smaller 'daughter' amoebas. These results demonstrate that the fluidity of the lipids can alter the morphology and dynamics of Min protein mesoscale structures.

One unique feature of this particular study on planar lipid bilayers is that it was performed with a controlled flow cell designed to maintain a constant supply of Min proteins in the solution phase above the membrane. This was done primarily to evaluate the validity of Turing-based models of Min protein oscillation, since in this system, there should be no local inhomogeneities in aqueous-phase MinD/E concentrations. Given that pattern formation was still observed under these conditions, these results provided strong evidence that changes in local MinD/E concentrations in solution are not required for pattern formation to occur. The authors propose that some other biochemically based timing mechanism must be involved in the generation of these patterns, and suggested a model that incorporated this idea with their observations. In their model the interaction of MinD dimers with the membrane surface may induce local membrane deformations that favors MinD polymerization. Different lipid membranes might be deformed to different

degrees, providing a potential mechanism for formation of the different structures observed with fluid versus more ordered lipid bilayers.

While it is known that interactions between MinD and the membrane are important in the Min protein cycle, it is not known how different membrane characteristics such as charge and fluidity may modulate MinD ATPase activity. This is particularly important since MinD ATP hydrolysis is the molecular switch that regulates Min oscillation, with slower rates of ATP hydrolysis being linked to slower rates of oscillation (10, 30). In addition, it is not clear how MinD preferentially initiates new polymerization events at the cell poles rather than the mid cell position. In this thesis I have started to address these questions by analyzing the influence of lipid bilayer conditions on MinE-stimulated MinD ATPase activity. Since ATP hydrolysis rates are linked to oscillation rates, with lower hydrolysis rates giving rise to slower or abnormal oscillation cycles (10), this can be considered to be an indirect measure of polymerization/depolymerization rates. The tools that I have developed for this purpose include kinetic assays of MinD ATPase function and a covalent modification assay to probe solvent accessible surfaces in the MinD polymer. In the following sections I will describe the basic theory behind each approach and how it will be applied to MinD.

1.7 MinD enzyme kinetics

Rates of ATP hydrolysis by MinD are typically measured by monitoring the increase in free inorganic phosphate (P_i) over time. In the initial phases of the reaction (i.e. less than 30% of substrate consumed), a plot of the phosphate concentration versus time should yield a straight line with a slope that represents the initial reaction rate (31). Moreover, since MinD activity depends on its interaction with MinE, kinetics can be used to probe the MinD-MinE interaction by measuring the rate of ATP hydrolysis as a function of MinE concentration. These rates can be used in an analysis based on the Hill equation to measure the apparent affinity of MinE binding to MinD (31), the standard form being given by;

$$\theta = \frac{[L]^h}{K^h_{0.5} + [L]^h}$$

where θ is the fraction of available MinE-binding sites in MinD that are occupied, the ligand L is MinE, $K_{0.5}$ is the concentration of MinE required to reach half-maximal activity, and h is the Hill coefficient, a measure of cooperativity. According to current models of MinD ATPase activity, MinE binding promotes ATP hydrolysis, leading to dissociation of the complex. Therefore according to this model, MinD ATPase activity is directly proportional to MinE binding, and all available MinE binding sites should be occupied when MinD activity has reached maximal levels. In this case the ratio of the initial rate (V_o) to V_{max} can be considered to represent θ to give:

$$\frac{V_o}{V_{max}} = \frac{[MinE]^h}{K^h_{0.5} + [MinE]^h}$$

According to this model $K_{0.5}$ provides a measure of the relative affinity of MinE for MinD whereas h is an indicator of the level of cooperativity of MinE binding and/or activation of MinD.

In addition to providing an indirect measure of the affinity of the MinE-MinD interaction, the kinetic parameters for MinE-stimulated MinD ATPase activity can be used to examine the influence of the lipid membrane on the Min cycle. In my thesis this assay will be used to investigate the influence of different physical properties of the lipid bilayer on maximal MinD activity (V_{max}), the MinE-MinD interaction ($K_{0.5}$), and MinD polymerization (h). Since differences in these parameters could be due to differences in the structure of extent of Min polymer formation, we would also like to develop a method that can be used to look for these changes in polymer structure.

1.8 Characterization of protein interaction surfaces in polymeric structures by chemical modification/mass spectrometry

Although kinetics will provide some insight into the effect of different lipid conditions on the functional status of MinD and its ability to be activated by MinE, it does not directly report on the morphology of the polymer. Consequently, if information on the Min polymer structure is to be obtained under the same conditions used to assay this function then it will be necessary to develop a complementary method. For this purpose, we are interested in characterizing the interaction surfaces that become buried upon polymer formation, since this could be different for the different types of polymers that are formed. In fact, there is no information yet available on the protein-protein interactions involved in higher order polymer formation. Therefore, we propose to probe the solvent-accessible surface of MinD using covalent chemical modification, and then monitor how this changes under conditions known to promote polymer formation. According to this strategy, chemically modified residues can be identified by proteolysis of the quenched reaction, followed by mass spectrometry (MS) of the peptide mixture. Comparison of peptide masses in the covalently modified mixture to those provided by a control mixture that did not undergo the labeling reaction can then be done to identify regions of the protein that undergo modification. Changes in accessible surface area that occur upon polymer formation identify regions of a protein that are important for the interaction. This technique has been used previously to characterize actin polymerization by G-actin proteins that form the F-actin microfilament upon nucleotide exchange with ATP (57). When the F-actin polymer was subjected to chemical labeling by oxidation followed by proteolysis, MS analysis of the peptide mixture showed that a total of 14 out of 26 peptides were protected from oxidation. Protected peptides located at the surface of the G-actin structure were therefore most likely to be involved in protein-protein interactions in the F-actin polymer.

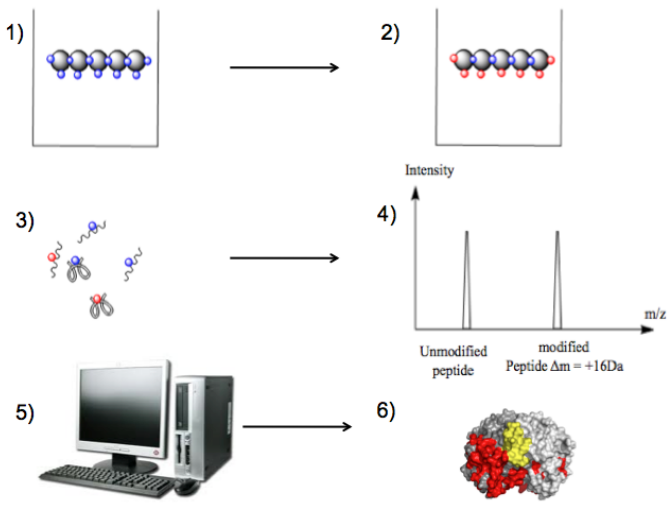

Figure 1.9: Schematic illustration of the covalent-modification approach to structural characterization of macromolecular complexes. *1) A polymeric protein sample is subjected to a labeling reaction to produce the sample in 2) with solvent exposed residues modified (red), but not those regions of the molecule buried in intermolecular interfaces (blue) The reaction is then stopped and subjected to digestion by protease to generate the peptide mixture shown in 3). Mass spectrometry of the peptide mixture produces the spectrum shown in 4). Subsequent steps include; 5) analysis of the spectrum to identify modified peptides using matching software such as Mascot (58), and; 6) mapping these peptides back to the protein structure. Peptides from solvent-exposed regions of the monomeric structure that show protection from the labeling reagent are more likely to be involved in direct interactions with other subunits in the polymer.*

One of the most general types of labeling reactions used to interrogate protein-protein interaction surfaces is the solvent deuterium exchange (HDX). In this experiment, exchangeable hydrogen atoms in the protein such as hydroxyl, sulfhydryl and amide protons can undergo an exchange reaction with solvent deuterium in D_2O (59). Backbone hydrogen atoms that are involved in hydrogen-bonded and/or buried structural elements will show a reduced rate of exchange compared to non-hydrogen bonded, solvent exposed sites (60). Since all non-proline amino acids have a similar intrinsic tendency to undergo this reaction, all parts of a protein sequence have the potential to be studied by this reaction. In addition, ionization efficiency of deuterated peptides is roughly similar that of the protiated analogue, allowing labeling efficiency to be accurately quantified by MS (60).

Although HDX has the advantage of being a very general method for labeling protein complexes, it can be difficult to find conditions that quench the reaction yet remain compatible with conditions required for analysis of the peptide mixture (61, 62). The HDX reaction can be quenched by low temperatures and low pH (60), requiring the use of robust proteases such as pepsin. However after digestion, these exchange-quenching conditions must be maintained while the peptide mixture is subjected to liquid chromatography (LC) followed by electrospray ionization (EI). Consequently, the HDX labeling method requires access to highly specialized equipment (typically custom-built) that would be capable of performing LC and EI at low temperatures. At this time there are not such instruments available in the Ottawa area.

To overcome the difficulties imposed by performing proteolysis and MS analysis under exchange-quenching conditions, irreversible covalent modifications can be used as a labeling reaction instead. Typical examples of this type of reaction include oxidation and glycation (63, 64). Oxidation is particularly attractive for more dynamic systems since the reaction is very rapid, with a broad range of potential modification sites. In this approach the reaction is performed by generating free radicals from oxygen, water or hydrogen peroxide. This can be done by electrochemical, photochemical, or radiolytic methods, or by using a catalyst as is done in the Fenton reaction (60). The latter reaction is particularly attractive as no special instruments or equipment are required for the reaction, unlike the other methods (63).

In the Fenton reaction highly reactive free hydroxyl radicals are generated from hydrogen peroxide by the oxidation of ferrous ions maintained in solution by chelating agents such as EDTA (65):

$$Fe^{2+} + H_2O_2 \longrightarrow Fe^{3+} + OH^- + {}^{\bullet}OH$$

Methionine and cysteine are the most reactive amino acids in this reaction, since they contain a sulfur atom that is a good target for hydroxyl radical attacks (60). As shown in Figure 1.10, methionine reacts with a hydroxyl radical to produce methionine sulfoxide (+16 Da) or methionine sulfone (+32 Da) (64). Upon oxidation, cysteine is

oxidized to sulfenic acid (+16 Da) or sulfonic acid (+32 Da). Aromatic amino acids such as tryptophan, tyrosine, phenylalanine and histidine can also react with hydroxyl radicals which attack the aromatic ring (66). Oxidation of aromatic amino acids results in formation of either carbonyl (+14 Da) or hydroxyl (+16 Da) groups in the side chain (67). It has also been shown that oxidation can cause amino acid conversion (e.g. histidine to asparagine, proline to glutamic acid semialdehyde) although the conditions required to achieve these conditions are usually much more extreme than are typically used in a protein labeling reaction (66, 68).

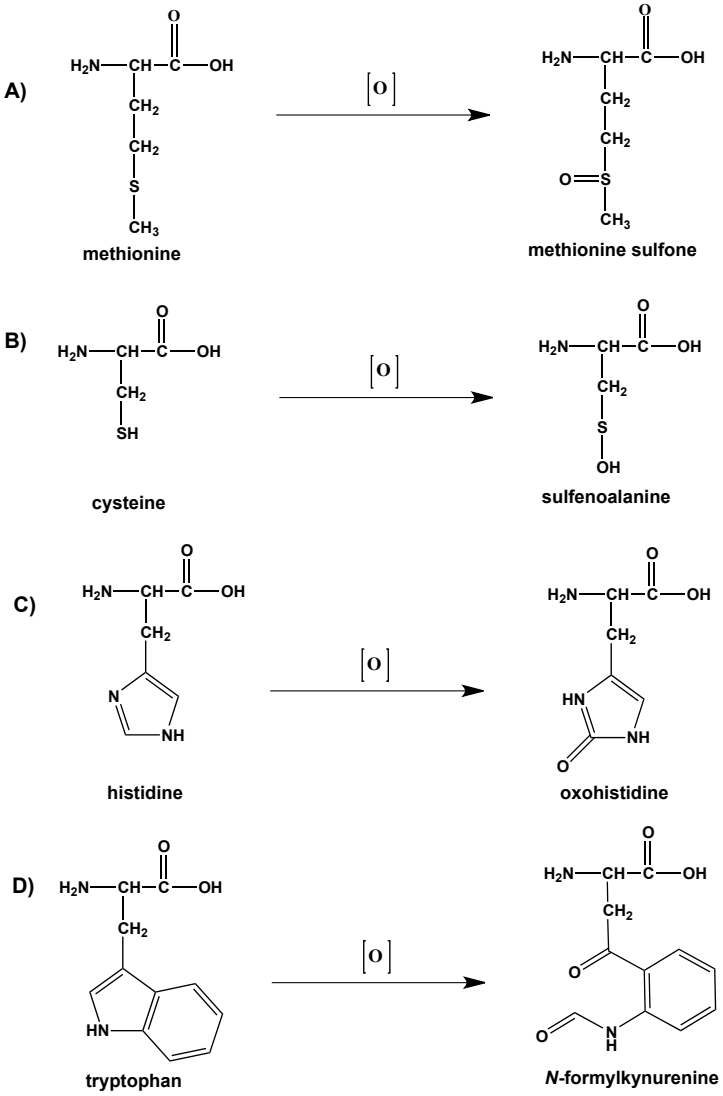

Figure 1.10: Examples of commonly observed oxidation reactions for amino acid side chains (69).

In this thesis, I have worked to develop a protocol that can be used to characterize the interaction surfaces in the MinD polymer using this oxidation reaction. This required that methods be developed for digestion of the reaction mixture by a protease, and subsequent detection and identification using mass spectrometry (MS). The two types of MS that were used in this thesis were matrix-assisted laser desorption/ionization (MALDI) and LC MS/MS. MALDI-MS requires that the sample be mixed with a matrix that can absorb energy from a laser beam to undergo ionization (70-72). The matrix can then transfer ions to the analyte, allowing desorption into the gas phase for detection according to its m/z ratio. A useful feature of MALDI is that it can be used to study intact proteins and in some cases will even allow the detection of higher order oligomers (< 500 kDa) (73).

The successful generation of informative MALDI MS spectra requires that samples be prepared with lower concentrations of salt, since their crystals can produce significant noise in the spectrum (70). When it is not possible to produce a peptide mixture with lower salt concentrations, LC MS/MS provides a convenient alternative, since the sample can be desalted and partially purified by liquid chromatography prior to electrospray ionization. Moreover, in the MS/MS instrument, it is possible to transfer a specific precursor mass to a chamber where collisions with gas molecules can be induced at energies sufficient to induce fragmentation (74, 75). The size of these fragments can be used to identify the composition of the precursor ion, and in many cases determine its sequence and/or sites of modification. Therefore, LC-MS/MS is the most frequent type of MS used to identify sites of covalent modification from the complex peptide mixture generated after proteolysis of the labeled complex.

1.9 Thesis objectives

Although some results have been published showing the influence of the lipid bilayer on MinD binding (47, 51), there have been no studies that evaluate the influence of various lipid bilayer characteristics on MinE-stimulated MinD activity, a central

component of the Min protein oscillation cycle. Previous work has identified a number of interesting features about MinD ATPase activity showing a very high degree of cooperativity for the MinE-MinD interaction, with less than 1:1 MinE to MinD being required for maximal activity (31). For these reasons our lab is interested in understanding how the properties of the lipid bilayer modulate MinD function. We are also interested in obtaining more structural information about the polymer in these different lipid environments. These goals gave rise to the following objectives pursued in this thesis:

- Characterization of the kinetic parameters of MinE-stimulated ATP hydrolysis by MinD.
- Investigation of the influence of the physical properties of the lipid bilayer on MinD ATPase activity.
- Development of a labeling protocol to identify the amino acid residues that are involved in MinD polymerization.

Results from this work will help elucidate the role of lipid bilayer characteristics such as charge and fluidity in modulating the MinD ATPase activity that is associated with the Min oscillation cycle. In addition, development of a protocol to identify amino acids in MinD involved in its polymerization will help to evaluate the hypothesis that differences in MinD ATPase activity may reflect changes in the extent and/or structure of MinD polymers. Ultimately this work will help to enhance our understanding of the mechanism of Min protein oscillation in bacteria, and identify effective strategies for its inhibition in pathogenic species such as *N. gonorrhoeae*.

Chapter 2: Material and methods

In this thesis, all chemical reagents used to conduct experiments were purchased from Bioshop unless specified.

2.1 Bacterial plasmids

Plasmids for overexpression of MinD and MinE, obtained from Fatima Hafizi, a graduate student in the Goto lab were derived from the pet30a vector (EMD Millipore) containing kanamycin antibiotic resistance for selective screening (76). Expressed proteins included the sequence LEHHHHHH at the C-terminus for the purpose of purification by nickel affinity chromatography. All Min plasmids were amplified and sequences confirmed at the Ontario Health Research Institute sequencing facility.

2.2 MinD and MinE plasmid amplification

E. coli DH5α $CaCl_2$ competent cells (Novagen) were transformed and plated on LB-agar plates (10 g/L tryptone, 5 g/L NaCl, 5 g/L yeast extract and 15 g/L agar) with 50 μg/mL kanamycin. One colony was used to inoculate 50 mL of sterile LB media (10 g/L tryptone, 5 g/L NaCl and 5 g/L yeast extract) in a 50 mL polypropylene Falcon tube (Fisher) with 50 μg/mL kanamycin, followed by shaking incubation in a thermal incubator (Fisher) overnight at 37 °C. The bacterial culture was centrifuged at 6,000 rpm for 15 minutes at 4 °C using a Beckman Coulter Avanti J-E centrifuge equipped with a JA 25.50 rotor. The pellet was stored at -20 °C. Plasmid DNA purification was carried out using the Qiagen Plasmid Purification Kit, essentially as per the manufacturer's instructions (3^{rd} edition, 2005). Purified DNA was further purified and concentrated using the Sigma GenElute^{TM} PCR clean-up kit (NA 1020), according to the manufacturer's instructions.

2.3 Transformation

E. coli $CaCl_2$ competent cell stocks of DH5α and BL21 obtained from Novagen were divided into 20 µL aliquots and immediately flash frozen in liquid nitrogen prior to storage at -80 °C.

Transformations were carried out using standard protocols (77). Briefly, one aliquot of competent cells was placed on ice, followed by addition of 2 µL of a 10 ng/µL solution of plasmid DNA and gently mixed by flicking the side of the tube. Cells were placed on ice and incubated for 30 minutes on a rocking platform (VWR scientific). The competent cells were then subjected to a heat shock step at 42 °C for 2 minutes, after which 200 µL of sterile LB media was added to these cells. The mixture was then allowed to grow on a Qmax 500 shaker (Fisher scientific) for 1 hour at 220 rpm and 37 °C. After the incubation, 200 µL of cells was plated on kanamycin selective LB-agar plate and allowed to grow overnight at 37 °C.

2.4 Min protein expression

Expression of Min proteins was carried out in M9 media (57 mM Na_2HPO_4, 22 mM KH_2PO_4 and 8.5 mM NaCl, 1 mM $MgSO_4$ (fisher), 0.1 mM $CaCl_2$ (fisher), 50 µg/ml kanamycin, 0.1% w/v NH_4Cl, 0.3% w/v D-glucose and 800 µL of 100x MEM vitamins (Gibco)) as previously described (78). In this method a single colony from freshly transformed BL21(DE3) cells was used to inoculate 80 mL M9 media. The culture was allowed to grow at 37 °C with shaking at 220 rpm for 16 hours. The culture was transferred into 800 mL M9 media and placed in a shaking incubator at 220 rpm, 37 °C for 2-3 hours. The culture was induced with 0.5 µM isopropyl β-D-1-thiogalactopyranoside (IPTG) once the OD_{600} reached 0.5-0.7. The culture was then allowed to grow for 4 to 5 hours at 37 °C or overnight at 16 °C until the OD_{600} was approximately ~1.0 – 1.4. Bacterial cells were harvested using an Avanti JE centrifuge at 4800xg at 4 °C for 10 minutes. The pellet from one 800 mL expression culture was divided into two 50 mL falcon tubes and stored at -20 °C. At different stages during the

growth a 1 mL sample was removed for SDS-PAGE analysis. These samples were centrifuged for 1 minute at 16000xg in table top Eppendorf 5415 D, and the pellet was suspended in 100 µL of sample loading buffer and stored at -20 °C until further analysis.

2.5 Min protein purification

A pellet obtained from 400 mL of expression culture was resuspended on ice in 15 mL lysis buffer (50 mM Tris-HCl pH 8.5, 250 mM NaCl and 10 mM imidazole) with 15 mg benzamidine added to the solution. After a 30 minute incubation on ice on a rocking platform, cells were sonicated on ice with a Fisher Scientific 500 Sonic Dismembrator for 3 cycles (1s on/1s off for 1 minute) at 45% amplitude, and allowed to incubate on ice for 1 minute between cycles. Cells lysates were then centrifuged at 16000xg for 20 minutes at 4 °C, using an Avanti J-E centrifuge equipped with a JA 25.50 rotor.

The supernatant was transferred to a 2.7 cm inner diameter column (Kimble) containing 5 mL Ni-NTA resin (Qiagen) that had been equilibrated with 5 mL lysis buffer. The supernatant was allowed to incubate on the column for 10 minutes. The resin was washed three times with 25 mL lysis buffer, washed twice with 25 mL washing buffer (50 mM Tris pH 8.5, 250 mM NaCl, 30 mM imidazole), and then incubated with 10 mL of elution buffer (37.5 mM Tris pH 8.5, 190 mM NaCl, 500 mM imidazole) for 5 minutes. Elution fractions were collected along with 2 additional 10 mL aliquots of elution buffer that were added to the resin to ensure complete recovery of bound Min protein. EDTA pH 8 was added to a final concentration of 0.5 mM for all elution fractions. After purification, nickel-NTA was washed with 25 mL ddH_2O followed by addition of 20% ethanol for short period storage.

The nickel-NTA resin was used for approximately 5 rounds of purification and then regenerated according to protocols outlined the QIAexpressionist handbook on nickel affinity chromatography (5^{th} edition). Briefly, the resin was washed with 2 volumes of regeneration buffer (6 M Gu-HCl and 0.2 M acetic acid), 5 volumes of

ddH_2O, 3 volumes of 2 % SDS, 1 volume each of 25%, 50% and 75% ethanol, followed by 5 volumes of 100% ethanol, then 1 volume of 75%, 50% and 25% ethanol. The resin was rinsed with 1 volume of ddH_2O, 5 volumes of 100 mM EDTA pH 8 and 1 volume ddH_2O. The resin was then charged with 2 volumes of 100 mM $NiSO_4$, and then washed with 2 volumes of ddH_2O, 2 volumes of regeneration buffer and 1 volume of ddH_2O before being transferred into lysis buffer.

Eluted protein was concentrated using Amicon Ultra concentration devices with a 10 kDa MWCO for MinE and 30 kDa MWCO for MinD by centrifugation at 3800xg using a Spinchron centrifuge (Beckman-Coulter) equipped with a S4180 hanging bucket rotor. After washing concentration devices with lysis buffer, eluted fractions were concentrated to a final volume of 4 mL. The concentrated sample was then transferred to a falcon tube and centrifuged for 2 minutes at 3,800xg in order to remove any aggregates that were present.

Samples were then subjected to size exclusion chromatography on a 10/300 Superdex 75 column (GE Healthcare) equilibrated with 50 mL (2 column volumes) size exclusion buffer (50 mM Tris-HCl pH 8.5, 100 mM NaCl and 0.2 mM EDTA). Chromatography was performed at 0.5 mL/min with 2 mL injections of concentrated protein per run, and 0.5 or 0.7 mL fractions collected during elution. Absorbance at 280 nm was used to record the elution profile.

25 µL samples of fractions acquired at each stage of the purification were retained and mixed with 25 µL of 2X sample loading buffer for SDS-PAGE analysis.

2.6: Determination of protein concentration

A 2 mg/mL stock of bovine serum albumin (BSA) from Fisher scientific was employed as the protein concentration standard in the bicinchoninic acid (BCA) assay (Pierce) (79, 80). Serial dilutions of the BSA stock were used to make 25, 50, 100, 200, 400, 500, 750 and 1000 µg/ml solutions in ddH_2O which were stored at 4 °C. The BCA

working solution was made by mixing 50 parts of reagent A (200 mM sodium carbonate, 120 mM sodium bicarbonate, 10 mM sodium tartrate, 0.1 M sodium hydroxide and 30mM bicinchoninic acid) with 1 part of reagent B (4% cupric sulphate). 1 mL of working solution was added to 50 µL of each standard and each unknown sample, whereas ddH_2O was used as a control (1:20 as working solution to sample or standard). Reaction mixtures were incubated for 30 minutes at 37 °C. Absorbance readings were obtained using Ultraspec 2100 pro UV spectrometer. Linear regression was performed to find the best fit line to the plot of absorbance versus BSA concentration, and the values from this equation used to convert absorbances from Min samples into protein concentrations.

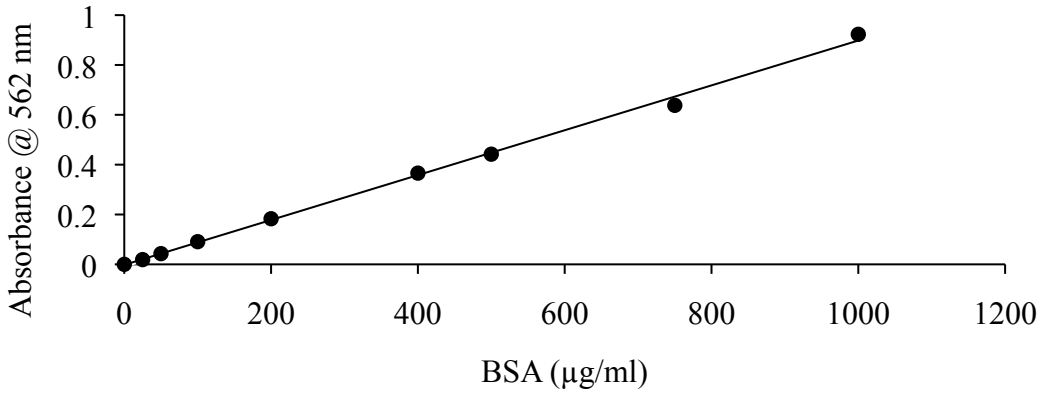

Figure 2.1: Representative sample of the BSA standard curve. *The line produced by linear regression with equation y=(0.0009 mL/mg)x +0.002 is shown (R^2=99.757%).*

2.7 Preparation of phospholipid vesicles

All lipids, such as those derived from *E. coli (total lipid extract)*, 1,2-dioleoyl-*sn*-glycero-3-phospho-(1'-*rac*-glycerol) (DOPG) and 1-palmitoyl-2-oleoyl-*sn*-glycero-3-phospho-(1'-*rac*-glycerol) (POPG) were purchased from Avanti Lipid. A 25 mg/ml lipid stock was transferred to glass test tube using a glass pipette. The chloroform was evaporated by a constant stream of argon for approximately 40 minutes, and then left in the fume hood overnight. The lipid film was suspended in 2.5 mL buffer containing 25 mM Tris-HCl pH 8 and 50 mM KCl followed by vortexing till completely dissolved

(final lipid concentration 10 mg/mL). Lipids were divided into eppendorf tubes and stored at -20 C°. Prior to use in the ATPase assay, lipids were allowed to thaw at room temperature and small unilamellar vesicles (SUVs) were made using a lipid extruder equipped with Hamilton 250 µL syringes (Avanti). A 0.1 µm polycarbonate filter was used for both DOPG and POPG. For *E. coli* lipid, the samples were first extruded through a 1 µm filter before extrusion with a 0.1 µm filter. The extruder was washed with ddH_2O prior to each extrusion to ensure there was no air in the device. LUV lipids stored at 4 °C and were good for 4 days.

Lipid type	Head group	Charge	T_m (C°)	Acyl chain specifications	Structure
DOPG	PG	negative	-18	(18:1)/(18:1) diunsaturated	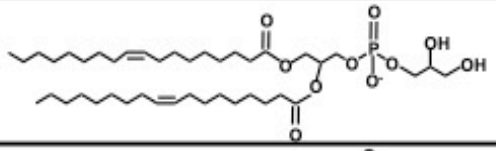
POPG	PG	negative	-2	(16:0)/(18:1) monounsaturated	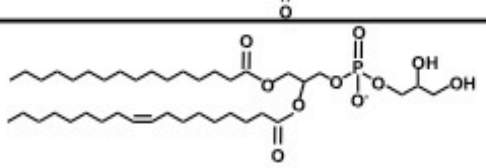
DOPC	PC	neutral	-20	(18:1)/(18:1) diunsaturated	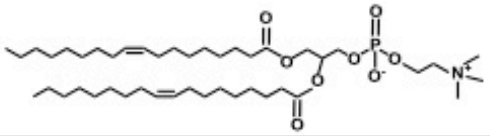
E. coli PE	PE	neutral	25	(16:0)/(18:1) monounsaturated	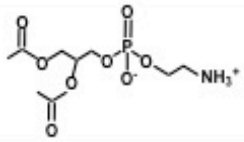
E. coli CL	CL	negative	35- 62	(15:0)/(18:cyclopropyl site) (18:1)/(16:0) Monounsaturated with Cyclopropyl site	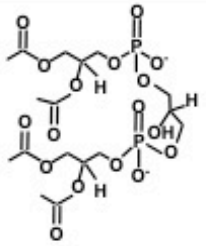
E. coli total	70% PG 20% PE 10% CL	negative	11-14		

Table 2.1: Summary of different lipid types used in this thesis. Lipid structural information was extracted from Avanti Lipid website. *Melting temperature (T_m), 1,2-di-(9Z-octadecenoyl)-sn-glycero-3-phospho-(1'-rac-glycerol) (DOPG), Phosphatidylglycerol (PG), 1-palmitoyl-2-oleoyl-sn-glycero-3-phospho-(1'-rac-glycerol) (POPG), 1,2-dioleoyl-sn-glycero-3-phosphocholine (DOPC), phosphocholine (PC), phosphatidylethanolamine (PE) and cardiolipin (CL). T_m values for CL and total lipid extract were estimated from (55, 56). The ratio represents (number of carbon atoms in given chain:modification such as number of double bonds found in given chain). Only headgroups are presented in PE and CL lipids.*

2.8 Malachite green working reagent for ATPase assay

One volume of 4.2% (w/v) ammonium molybdate (Aldrich) in 4 M HCl was mixed with three volumes of 0.045% (w/v) malachite green (Bioshop), vortexed, and then incubated on a shaking platform for 1 hour at room temperature. The solution was filtered with a 0.22 µm MF-millipore membrane to trap particulates, and then stored at 4 C°. Just prior to the ATPase assay, Tween-20 was added to a final concentration of 0.15% (v/v), and incubated on a rocking platform for 1 hour at room temperature.

A standard curve for malachite green was constructed using potassium phosphate. The standard curve was linear to a maximum quantity of ~8 nmol, well above the maximum amount of phosphate typically produced in the MinD ATPase assay (~1.2 nmol). The best-fit line to the linear portion of the standard curve was found to be y= (0.277±0.00075 $nmol^{-1}$)x+0.0713±0.0033, (R^2 = 99.7±0.0016%), with the slope providing the conversion factor to calculate the amount of phosphate produced during an ATPase assay.

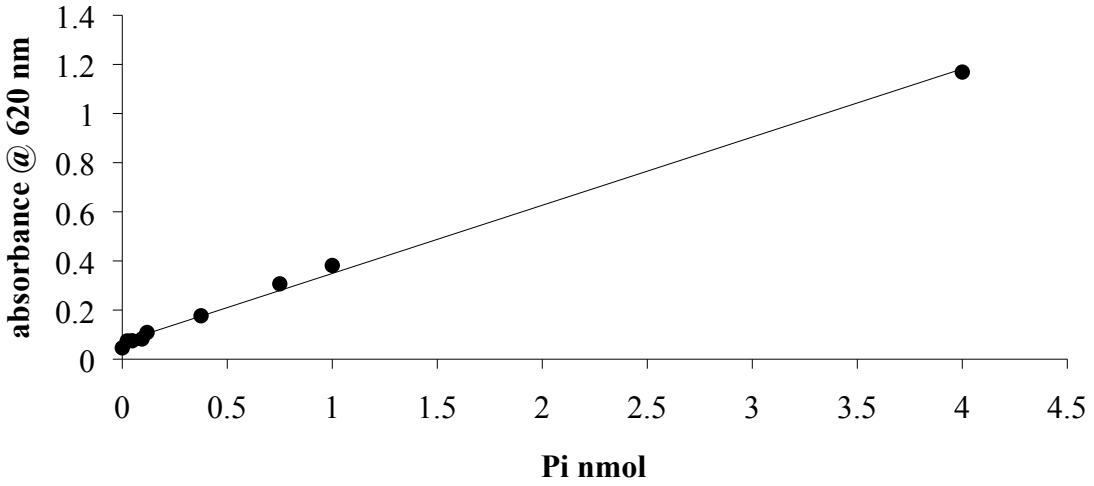

Figure 2.2: Standard curve for malachite green assay constructed using potassium phosphate. *15 µL of each sample was added to 70 µL the malachite green solution. The reaction mixture was incubated for 15 minutes at room temperature and the optical density was measured at 620 nm.*

2.9 MinD ATPase assay

MinD ATPase assays were run in 65 mM Tris-HCl pH 8.2, 80 mM NaCl, 50 mM KCl, 0.16 mM EDTA, 5 mM $MgCl_2$, 0.5 mg/ml phospholipid, and 1 mM ATP (Fermentas). MinD and MinE concentrations (3 μM and 1 – 3 μM, respectively) chosen for these assays were based on previous estimates of Min protein concentrations in *E. coli* (30, 81). Unless otherwise stated, ATP was the last component added to each reaction. 40 μL aliquots of were removed at each time point and subjected to a boiling water bath for 1 minute (except for late phase measurements performed with DOPG). Samples were centrifuged in a table top Eppendorf 5415 D at 16000xg for 4 minutes. 15 μL of the supernatant was mixed with 70 μL of malachite green in a clear polypropylene 96-well microplate and incubated at room temperature for 15 minutes. Optical density values at 620 nm were quantified on a SPECTRAmax PLUS^{384} Microplate Spectrophotometer. The absorbance of each sample was plotted as a function of time, giving rise to a linear relationship, with the slope proving a measure of the initial rate of ATP hydrolysis. Rates were converted into phosphate concentrations, and normalized to MinD mass (in mg) to determine the specific activity. Error bars in activity represents the standard error calculated from the average of three different trials with different MinD preparations.

2.10 SDS-PAGE analysis

SDS-PAGE was performed using the Laemmli procedure (80). Samples to be analyzed were added to 2x sample loading buffer (125 mM Tris pH 6.8, 20% (v/v) glycerol, 4% (w/v) SDS, 0.01% (w/v) bromophenol blue and 2% (v/v) metacaptoethanol (Sigma)). The mixture was then incubated in a boiling water bath for 5 minutes. Samples and EZ-Run protein marker (Fisher) were loaded into pre-cast polyacrylamide gels with 4% stacking phase and 12% resolving phase (Peirce) and run in a PROTEAN electrophoresis cell (Biorad) for 40 minutes at 150 mV in running buffer (100 mM Tris pH 8, 100 mM HEPES and 1% (w/v) SDS.

The gel was stained by Coomassie blue stain (50% (v/v) methanol, 10% (v/v) acetic acid and 0.1% (w/v) coomassie brilliant blue) for 30 minutes on a rocking platform. This was followed by incubation in destaining solution (50% (v/v) methanol, 10% (v/v) acetic acid) for 1 hour, followed by another hour of incubation in fresh refreshing the destaining solution. Gels were stored in ddH_2O prior to scanning on a flatbed scanner (Epson).

2.11 MinD oxidization reaction

Control and test reactions were preformed in glass test tubes with 0.5 mL 6 μM [MinD], 0.5 mg/ml phospholipids, 5 mM $MgCl_2$, which had been incubated for a minimum of 10 minutes at room temperature after addition of ATP to 1 mM concentration. In the oxidation test, ferrous ammonium persulfate (supplying both the iron catalyst and the radical reaction initiator) and EDTA, pH 8 (to keep the iron in solution) were both added to a final concentration of 0.5 mM, followed by incubation with 0.3% H_2O_2 (Sigma) for 3 minutes (82). Reactions were transferred to 45-90 μm diameter chromatography columns equipped with filters (Evergreen) containing 150 μL of nickel-NTA resin pre-equilibrated in size exclusion buffer. Oxidation reactions were quenched by washing 3 times with 30 μL of ice-cold 50 mM Tris pH 8. MinD was eluted into 1.5 mL Eppendorf tubes using 100 μL 250 mM imidazole pH 8.5. On some occasions, when it was necessary to perform the reaction on smaller reaction volumes (<40 μL), elution was assisted by brief (2 – 5 seconds) centrifugation in a tabletop centrifuge.

2.12 MinD-Tryptic digestion

One volume of immobilized trypsin (Promega) (10 μL, containing 60 units) was washed three times with 4 volumes (40 μL) of 50 mM ammonium bicarbonate (pH 7). 60 μL of eluted MinD protein from the nickel affinity purification step following oxidation (Section 2.14) was added to the equilibrated immobilized trypsin in an eppendorf tube,

and incubated at room temperature for 5 minutes. The resin was allowed to settle and the supernatant containing the peptide mixture was transferred to a new eppendorf tube.

The peptide mixture was purified and concentrated with a ZipTip® (Millipore) equipped with C_4 resin (spherical silica, 15 μm and 300 Å pore size). The resin was washed with 10 μL 100% acetonitrile (wetting solution) and equilibrated with three washes of 0.1% TFA (Sigma). The tip was then immersed in the peptide mixture and 10 μL was pipetted through the resin at least seven times to maximize binding. The resin was then washed with 10 μL of 5% methanol and 0.1% TFA, and peptides eluted by pipetting 10 μL of elution solution (50% methanol and 0.1% formic acid) in a fresh tube at least seven times through the tip.

2.13 MALDI spectrometry

To prepare samples for MALDI spectrometry, sinapic acid (Sigma) was dissolved in 75% acetonitrile and 0.01% formic acid to the point of saturation. The solution was centrifuged for few seconds in order to pellet undissolved sinapic acid.

One volume of peptide or protein sample was mixed with one part sinapic acid solution, and 1 μL of the mixture was spotted on 96 MSP polished steel MALDI target (Bruker) and dried at room temperature. Experiments were done using a Bruker microflex MALDI-TOF mass spectrometer with laser intensity set to 75% for 200 shots, with a frequency of 60 Hz.

Chapter 3: Results

3.1 Overexpression and purification of MinD and MinE

C-terminally hexahistadine tagged MinD and MinE proteins were overexpressed in *E. coli* BL21 (DE3) competent cells and purified by nickel affinity chromatography, as previously described (83, 84). As shown in Figure 3.1, samples collected at various stages during the course of purification by nickel affinity chromatography showed a band with the mobility expected for either MinD or MinE, with a single band in the final eluted product. Since the imidazole used to elute Min proteins interferes with reagents used in the ATPase assay (85), a final purification step using size exclusion chromatography was performed, yielding samples that were more than 90% pure as assessed by SDS-PAGE.

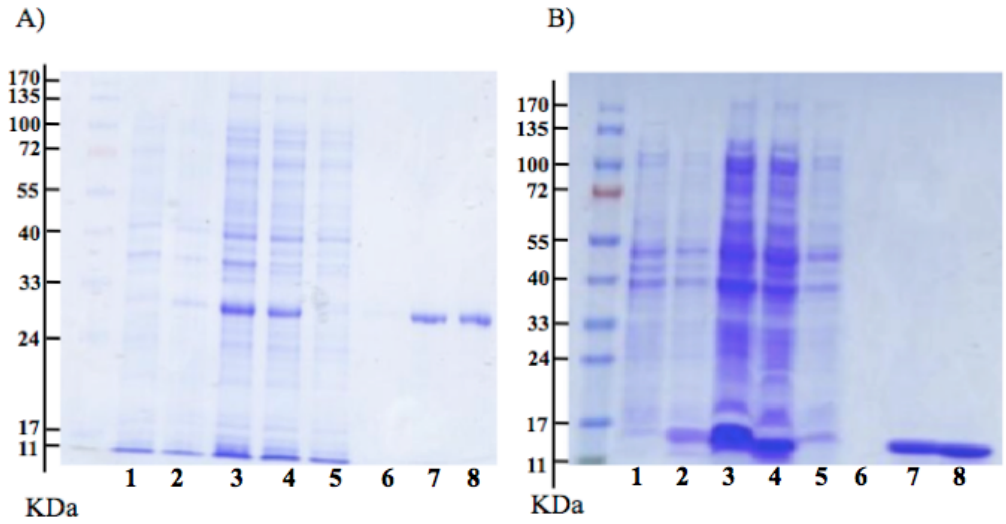

Figure 3.1: SDS-PAGE analysis of fractions taken from purifications of MinD (A) and MinE (B). *Lanes contain a sample from the bacterial culture before induction (lane 1), and after induction with IPTG (lane 2), cell lysate after sonication (lane 3), and supernatant after centrifugation (lane 4). Fractions taken from the nickel affinity chromatography purification show the lysis buffer wash (lane 5), 30 mM imidazole wash (lane 6), and 500 mM imidazole elution (lane 7). The purified sample obtained from size exclusion chromatography is shown in lane 8. The expected MW for $MinD_{Ng}$ is 30.7 kDa and for $MinE_{Ng}$ is 11.0 kDa.*

3.2 Stimulation of MinD ATPase activity

To confirm that functionally active MinD had been isolated, ATPase activity was assayed *in vitro* as previously described (19, 30, 31). As expected, no MinD activity was observed in the absence of Mg^{2+}, DOPG phospholipids or ATP, since these are all essential components for the reaction (30). A low rate of ATP hydrolysis by MinD was observed in the absence of MinE, consistent with the known basal activity of MinD. Upon addition of MinE, ATP hydrolysis rates increased by factor of 10-fold over rates obtained in the absence of MinE.

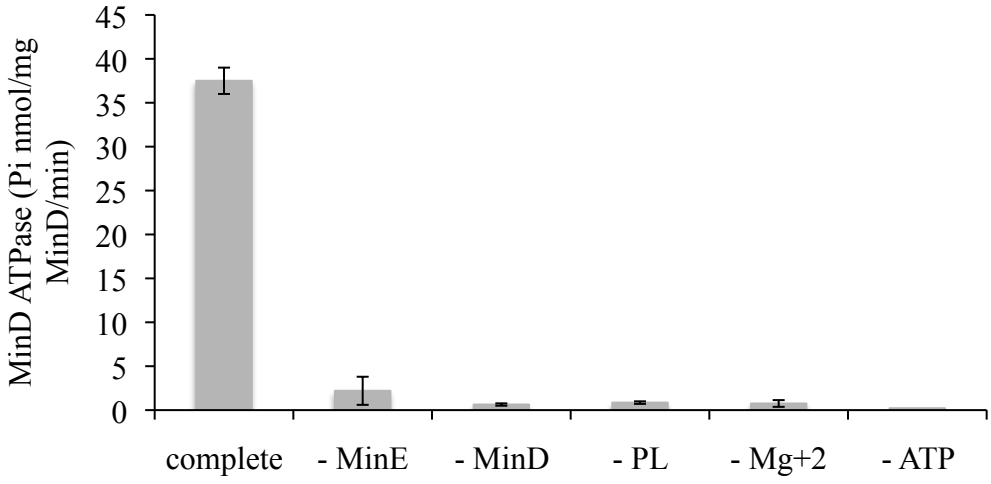

Figure 3.2: Confirmation of MinD ATPase activity in vitro. Maximal rates of ATP hydrolysis by MinD requires MinE, ATP, phospholipid and $MgCl_2$. *Control reactions missing one of the essential elements required for the reaction are indicated with the minus signs. All reactions were run with 2.7 μM MinD and 3 μM MinE in 65 mM Tris, pH 8.2, 80 mM NaCl, 50 mM KCl, 0.16 mM EDTA, 5 mM $MgCl_2$, 0.5 mg/ml DOPG small unilamellar vesicles and 1 mM ATP.*

3.3 Kinetic profiles for MinD ATPase activity on DOPG bilayers

In previous studies we have used the MinD ATPase assay to probe the interaction between MinD and MinE by measuring ATP hydrolysis rates as a function of MinE concentration, which could then be fit to the Hill equation. Specifically, it was used to evaluate the impact of MinE mutations on ATP hydrolysis, allowing identification of residues important of the stimulation of MinD ATPase activity (31). As another confirmation of the sample integrity I performed the same analysis for wild-type MinD on DOPG vesicles, and obtained values of 37.5±1.5 (nmol/mg MinD/min) for V_{max}, 0.11±0.02 μM for the concentration required for half-maximal activity ($K_{0.5}$) and 2.9±0.3 for the Hill coefficient (Fig. 3.3), which is in good agreement with previously determined values.

Although these assays provided important new insights into the interaction between MinD and MinE, we noticed an unusual feature in the rate profiles. In these assays, the Malachite green colorimetric assay was used to measure phosphate concentrations, with four different time points (2, 15, 28 and 41 minutes) typically being sampled for each reaction. Although the presence of MinE should not change the amount of phosphate present at time t=0, extrapolation of the initial rate profiles to the start of the reaction showed an increase in the amount of phosphate present at the start of each reaction. In other words, these reactions did not converge to the same initial phosphate concentrations at time t=0, as would be expected if the reaction rates were constant. This suggested that the rate of hydrolysis early in the reaction phase may be higher than that measured at a later phase in the reaction, a hypothesis we were interested in evaluating by monitoring the reaction at earlier time points.

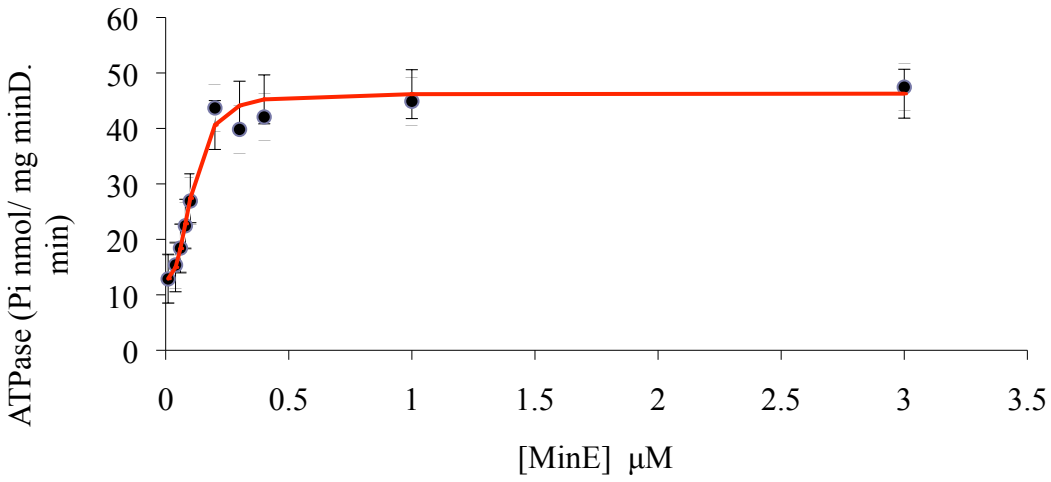

Figure 3.3: MinD ATPase rate profile as a function of MinE concentration fit to the Hill equation. *MinD ATPase rates with DOPG vesicles measured using previously published assay protocols (86). The best fit to the Hill equation shown (red line) gave a Vmax of 37±1.5 nmol of phosphate/mg MinD/min, $K_{0.5}$ of 0.11±0.02 mM and a Hill coefficient of 2.9±0.3.*

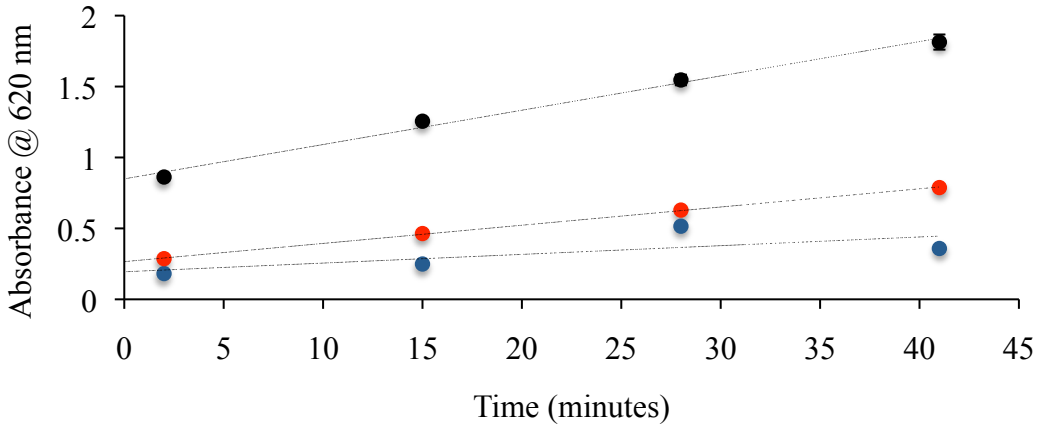

Figure 3.4: Representative initial rate profiles for MinE-stimulated MinD ATPase activity used to generate the kinetic profile in Fig. 3.3*. Different concentrations of MinE, 0.01 μM (blue), 0.1 μM (red) and 0.5 μM (black) were included in each reaction. Aliquots were taken after 2, 15, 28 and 41 minutes. Samples were centrifuged for 4 minutes at 16000xg, followed by incubation with the malachite green colorimetric reagent for 15 minutes, and absorbance at 620 nm measured. As shown by the extrapolations to t=0, the initial phosphate concentrations at time zero appears to increase as MinE concentration is increased. Standard error bars are smaller than the size of symbols.*

3.4 Assay modification to capture the early phase of the reaction

In order to obtain rate profiles from earlier parts of the reaction it was necessary to develop a method that could stop the reaction in a rapid and irreversible manner. In the established form of this assay the reaction mixture was centrifuged for 4 minutes at 16000 xg, under the assumption that this would remove membrane-bound MinD from the soluble phase, with remaining soluble MinD being inactive. Nonetheless, it is likely that MinD-catalyzed ATP hydrolysis occurred throughout this process. Moreover, since some vesicles may not have been large enough to sediment under these conditions, removal of the pellet fraction containing membrane-bound MinD would not have guaranteed that the reaction was completely inhibited. Therefore an alternate method to halt the reaction needed to be developed to allow earlier phases of the reaction to be monitored.

Previous studies had shown that MinD denatured when it was subjected to temperatures exceeding ~60 °C (87), suggesting that brief exposure to high temperatures could inactivate MinD. However, in order to use this approach it was necessary to confirm that ATP hydrolysis did not occur under MinD-inactivating conditions. For this purpose, ATP hydrolysis in protein-free buffer under elevated temperatures was measured for various incubation periods. As shown in Figure 3.5, incubation of ATP in a boiling water bath for 1 minute did not cause the release of phosphate beyond background levels, although exposure for longer periods (~5 minutes) did show some evidence of hydrolysis. These results suggested that a one-minute exposure to 100^{o}C could be tolerated in the ATPase assay.

To determine whether the MinD ATPase assay would be affected by a one minute exposure to denaturing conditions, the assay was performed using either centrifugation or heat denaturation to stop the reaction. As shown in Figure 3.6, there was no significant difference in measured MinD ATPase activity between the two methods, demonstrating the compatibility of the heat denaturation step with the assay.

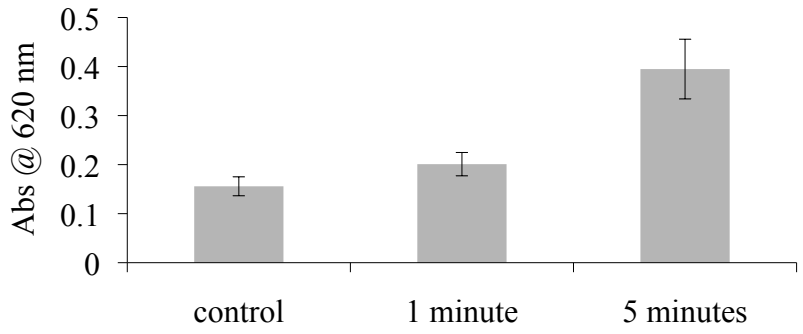

Figure 3.5: ATP thermostability test*. 1 mM ATP in size exclusion buffer (50 mM Tris-HCl pH 8.5, 100 mM NaCl and 0.2 mM EDTA) was incubated in a boiling water bath 0 (control), 1, or 5 minutes, and the amount of released phosphate monitored by absorbance at 620 nm in the malachite green assay.*

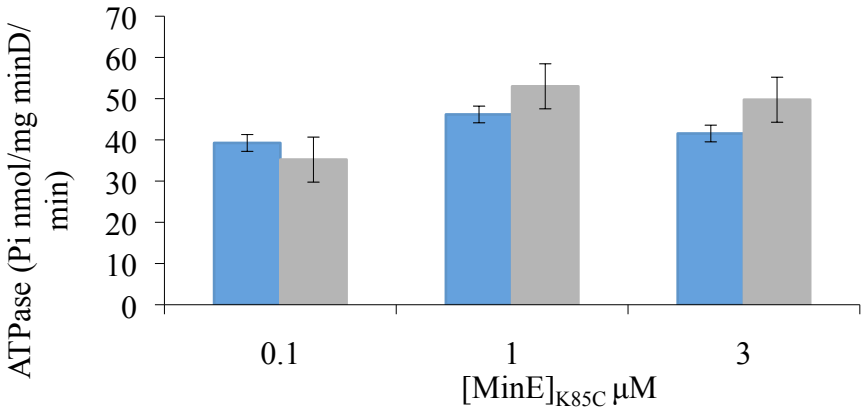

Figure 3.6: MinD ATPase activity measured with (grey) or without (blue) 1 min exposure to denaturing conditions prior to centrifugation. *These assays were performed with wild type-like $MinE_{K85C}$, which was the MinE protein available at the time for this assay. Reaction conditions are as described in Figure 3.2.*

3.5 Investigation of the early phase of MinD activity

Since our previous measurements of MinD ATPase activity suggested that the rate at earlier stages of the reaction may be faster than the rates measured at later stages in the reaction (i.e. > 5 minutes after initiation), we used the heat denaturation method to measure rates over the first three minutes of the reaction. As presented in Figure 3.7, the phosphate concentrations increased linearly over time, with a slope that increased with

increasing MinE concentration. Notably, the magnitude of the slope tended to be larger than that obtained when later points in the reaction were sampled for the rate measurement (e.g. Fig. 3.4) Also, unlike the previous initial rate profiles, extrapolation back to initial phosphate concentrations at time t=0 showed good convergence, as would be expected for a reaction with a constant rate over this time interval.

These data all suggested the existence of two different activity phases for MinD with DOPG, with a fast 'early' phase followed by slower 'late' phase. To confirm the presence of these two phases, MinD ATPase activity was monitored over a period that would be expected to span both early and late phases. As shown in Figure 3.8, the profiles showed good linearity during first ~5 minutes of the reaction and then leveled off to a new, slower rate as the reaction progressed. The difference between early and late-phase measurements was more apparent for reactions using higher concentrations of MinE. Similar results were also obtained if the reactions were diluted prior to addition of the malachite green reagent (Appendix, Fig. A1). This indicates that the plateau was not due to depletion of the malachite green reagent or deviations from Beer's law at the higher phosphate concentrations. Hence the differences in early and late phase measurements appear to reflect differences in the functional properties of MinD at different stages of the reaction.

Since the initial rates obtained in the early phase of the MinD reaction were different from those previously determined from sampling later points in the reaction, we were interested in evaluating the kinetic parameters of the early phase using the Hill equation. This profile is shown in Figure 3.9 using initial rates obtained from early-phase measurements only. Most striking is the maximal ATPase rate, which was found to be 245±29 (nmol/mg MinD/min), which is 6-fold higher than that found when measurements were obtained from the late phase. In addition, $K_{0.5}$ was found to be 0.45±0.12 μM, which is ~4-times higher than what was observed in the late phase, reflecting a lower apparent affinity for the MinD-MinE interaction. One of the possible explanations for this reduction in affinity may be that there are changes in the MinD

polymeric structure between early and late phases, potentially giving rise to different activation profiles.

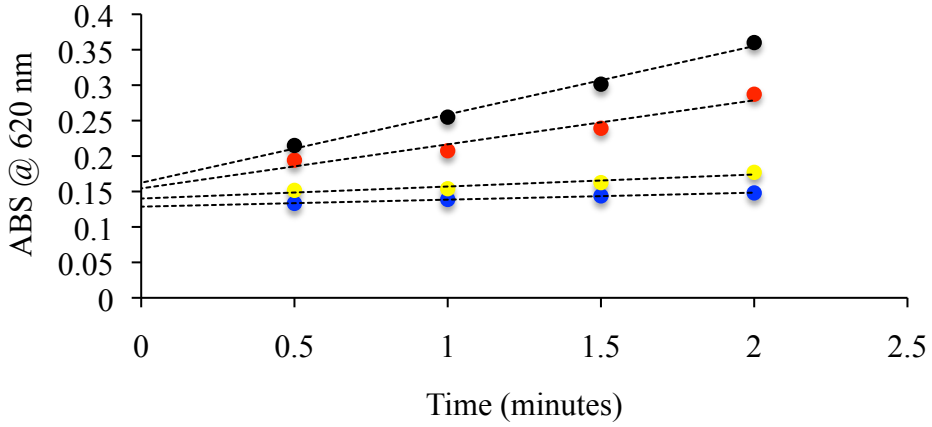

Figure 3.7: Initial rate profiles sampling the first two minutes of MinE-stimulated MinD ATPase activity using DOPG phospholipid. *Control 0 μM, (blue), 0.1 μM (yellow), 0.5 μM (red) and 1 μM (black) concentrations of MinE. Aliquots were taken after 0.5, 1, 1.5 and 2 minutes and subjected to a boiling water bath for 1 minute prior to centrifugation for 4 minutes at 16000xg and color development using the malachite green assay.*

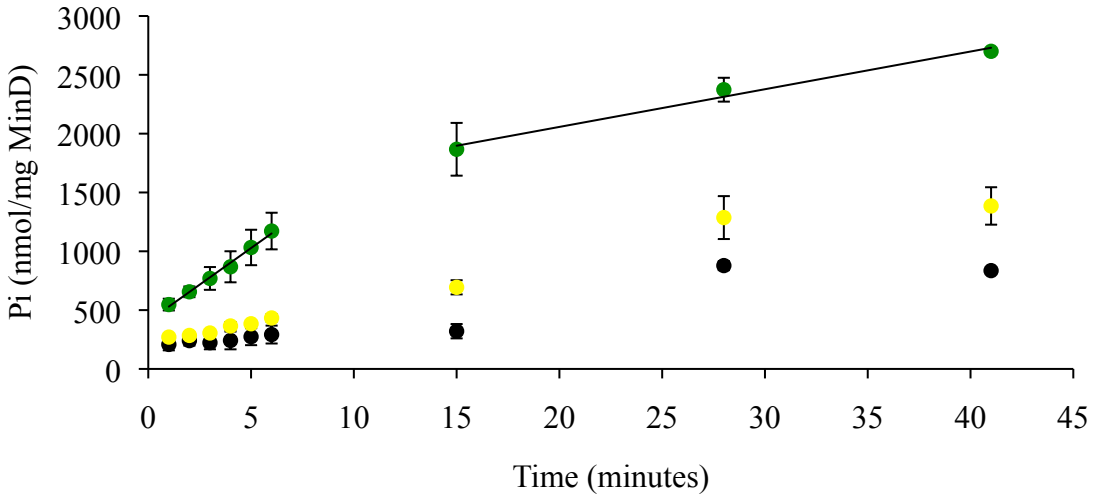

Figure 3.8: Rate profile for MinE-stimulated MinD ATPase activity with DOPG spanning both early and late phases*. Reaction conditions as described in figure 3.2 containing 0 mM (black), 0.06 μM (yellow) and 1.1 μM MinE (green).*

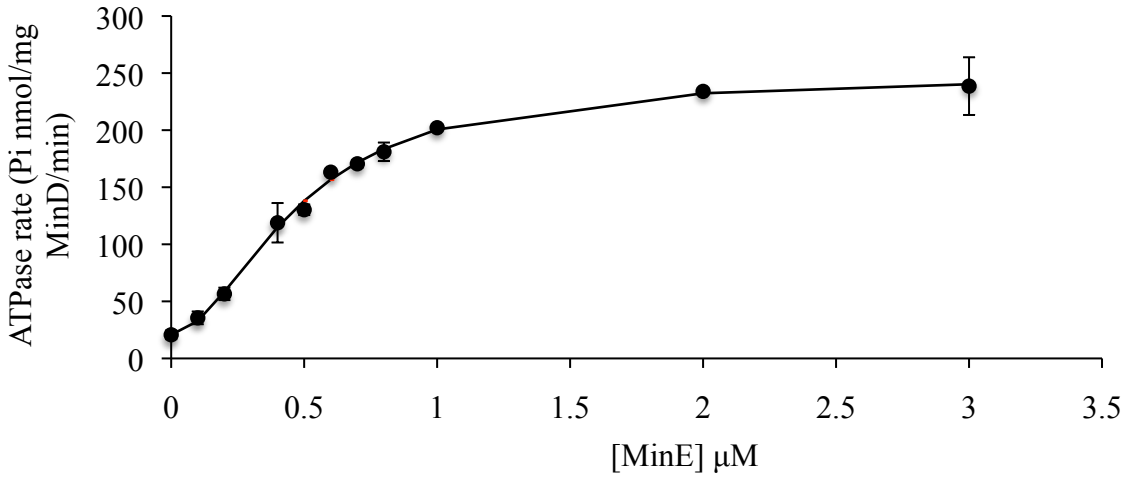

Figure 3.9: Kinetic profile for MinE-stimulated MinD ATPase activity based on initial rate measurements from the early phase in DOPG. *All rates were measured over 3 minutes time period using heat denaturation to stop the reaction. Hill equation parameters giving rise to the best fit to the experimental data (red line) are 245±29 P_i nmol/mg MinD/min for V_{max}, 0.45±0.12 mM for $K_{0.5}$ and 2.00±0.07 for h.*

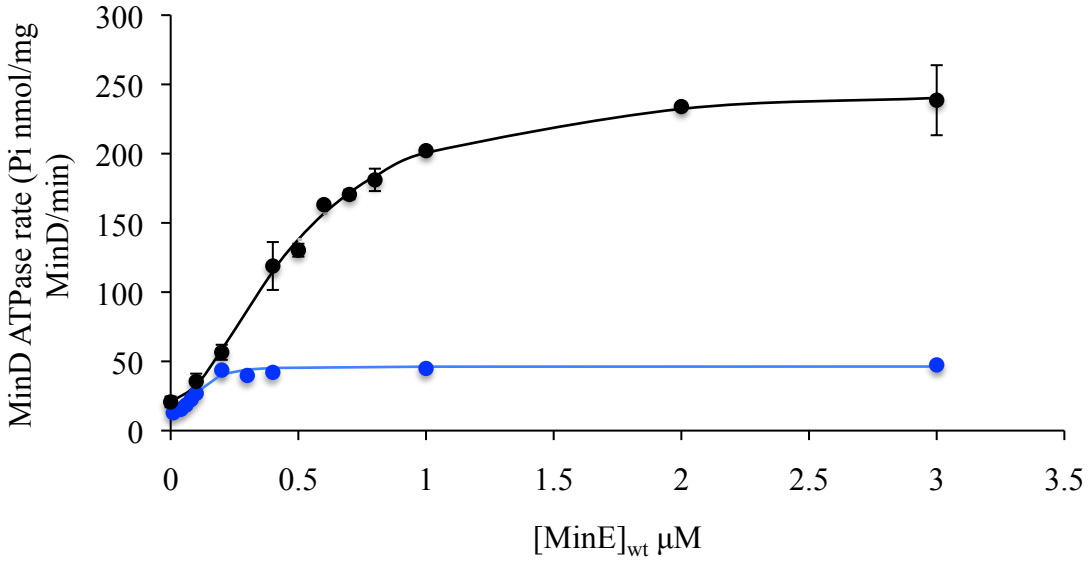

Figure 3.10: Comparison of MinE-dependent rate profiles obtained from early-phase (black), and late-phase (blue) measurements.

3.6 Investigation of the potential influence of MinD polymerization on ATPase rates

A potential explanation for the difference in kinetic behavior between the early and late phases of the reaction is that there is a difference in the properties of the MinD oligomer at different points in the reaction. These differences can alter the intrinsic ability of MinD to catalyze ATP hydrolysis, or may simply alter the number of binding sites that MinE can access to stimulate ATP hydrolysis. Given the fact that ATP was the last reagent added to the reaction, we hypothesized that the number of available MinE-binding sites might be large at the beginning of the reaction when the polymer has not had much time to form. However, as the polymer structure develops into a larger steady-state assembly, the number of accessible binding sites on the MinD polymer may decrease.

To test this hypothesis, MinD reactions were set up with no MinE and allowed to incubate for different times prior to addition of MinE. According to previous demonstrations of MinD polymer formation, incubation of MinD with lipid vesicles and ATP for ~10 minutes is proposed to be sufficient for polymer formation *in vitro*, with addition of MinE bringing about a dramatic reduction in the size and organization of the polymer (41). However, as shown in Figure 3.11, preincubation of MinD with ATP and DOPG vesicles did not change the initial rate of ATP hydrolysis measured during the early phase of the reaction. This suggests that MinE is required for the formation of these two different kinetic phases, and that MinD polymer formation in the absence of MinE does not affect this behavior. However, we cannot rule out the possibility that the conditions used to stimulate polymer formation prior to addition of MinE failed to promote MinD polymerization, particularly since it has not been shown that MinD forms a polymer in the absence of MinE at the lower protein to lipid ratios used in our assay.

Since the fraction of MinD expected to exist in a polymeric state should be a function of MinD concentration, we also repeated the initial rate measurements for a lower concentration of MinD. This suggests that MinD polymerization may not be responsible for the functional differences that were observed between early and late

phases. Alternatively, both MinD concentrations may have been far above the dissociation constant, with undetectable differences in polymer structure between the two conditions.

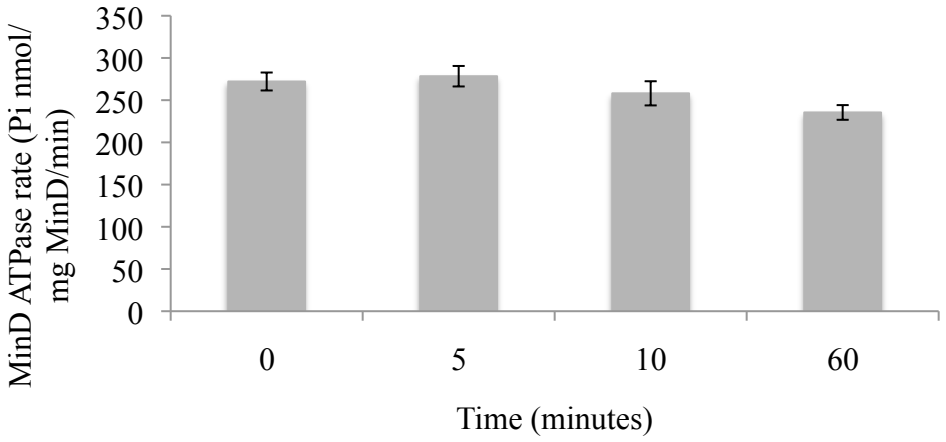

Figure 3.11: The effect of preincubating MinD with ATP and DOPG vesicles on MinD activity*. In order to promote MinD polymer formation prior to the addition of MinE, 2.7 µM MinD was pre-incubated with 1 mM ATP, 5 mM $MgCl_2$ and 0.5 mg/ml DOPG at room temperature for the indicated amount of time. MinD activity was then stimulated by the addition of 1 µM MinE and the initial rate of phosphate production over the following three minutes was measured. No statistically significant difference was observed between ATPase rates measured for the reaction that did not undergo pre-incubation versus those that did (two-tailed $p>0.05$) although $p=0.06$ between the $t = 0$ and 60 minute experiments.*

3.7 MinD ATPase activity on *E. coli* phospholipids

One possibility that could explain the differences in MinE-stimulated MinD activity in early and late phases is that the properties of the lipid were altered by MinE and MinD, and that this affected the functional properties of MinD. This suggested that properties of the lipid bilayer could be important in determining the kinetic behavior of MinD. Therefore, in order to gain a better understanding to how MinD behaves under more physiological conditions, late phase initial rate measurements were performed for *E. coli* lipid vesicles in place of DOPG. These results showed different kinetic properties compared to those obtained using DOPG, with $V_{max} = 20\pm3$, $K_{0.5} = 0.020\pm0.004$ and $h = 2.5\pm0.2$. This represents a 2 fold lower maximal activity and 5-fold stronger apparent

binding affinity on *E. coli* lipid relative to DOPG. These findings demonstrate that the lipid identity has a significant influence on the observed kinetic profiles for MinE-stimulated MinD activity.

To determine whether an early faster kinetic phase was also possible with a more physiologically relevant lipid mixture, a complete initial rate profile was measured, with phosphate concentrations being sampled every 30 seconds during the first 5 minutes of the reaction (Fig. 3.13). In contrast with the profiles obtained with DOPG, there was good linearity over the entire range, even when high concentrations of MinE were used. Therefore, it appears that there is no kinetically distinct early phase of the reaction when *E. coli* vesicles are used. In addition, previous studies with *E. coli* MinD assayed on *E. coli* vesicles displayed a ~5-minute period of inactivity in the beginning of the reaction when low concentrations of MinE were used under lipid tubule forming conditions (32, 41). However, we were unable to observe this lag phase under lipid tubule-promoting conditions (Fig. A2).

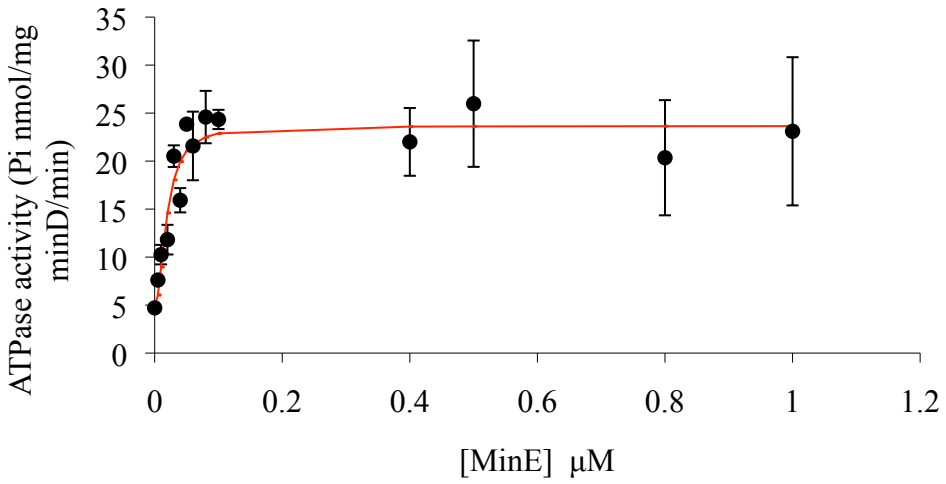

Figure 3.12: Kinetic profile for MinE-stimulated MinD ATPase activity with E. coli lipid using late-phase intial rate measurements. *All reactions contained 2.7 µM MinD, 1 mM ATP, 5 mM $MgCl_2$ and 0.5 mg/ml E. coli lipid. Aliquots were taken after 5, 15, 28, 41 minutes, boiled for 1 minute, and then analyzed using the malachite green assay. Parameters giving rise to the fit shown in this graph (red line) are: V_{max} = 20±3, $K_{0.5}$ = 0.020±0.004 mM and h = 2.5±0.2.*

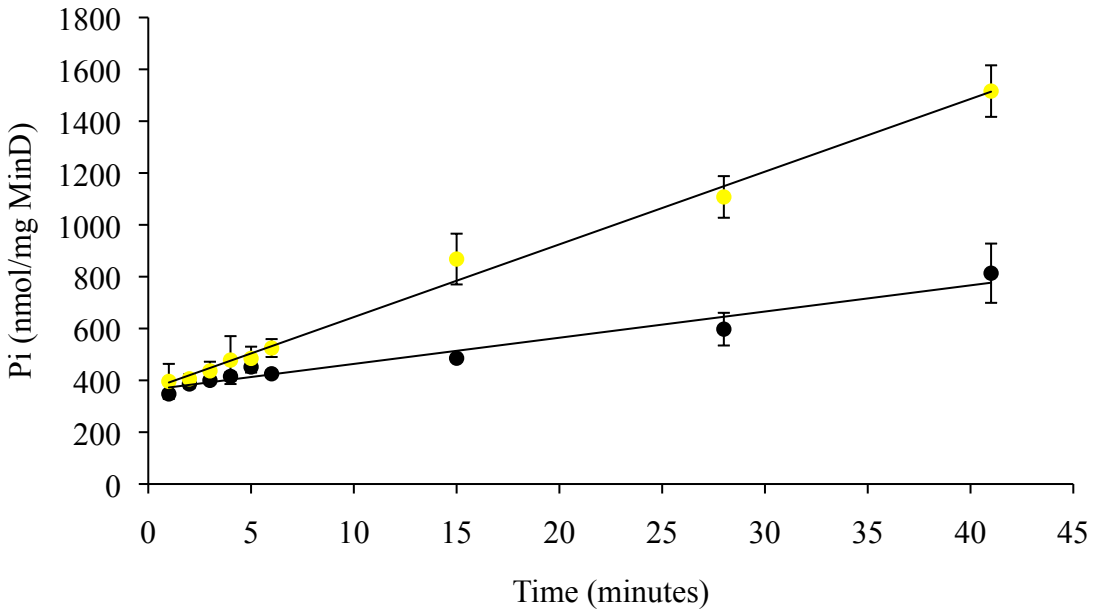

Figure 3.13: Initial rate profile spanning early and late phases of MinE-stimulated MinD ATPase activity with E. coli phospholipid. *Reaction conditions are as described in Figure 3.2 with 0 μM (black) and 0.1 μM (yellow) MinE.*

3.8 MinD ATPase activity on DOPC phospholipids

One of the characteristics of the DOPG lipid that may have been important for the observed kinetic properties is the anionic headgroup. In order to evaluate the impact of this negative head group charge on MinD function, SUVs made from the zwitterionic phosphocholine lipid DOPC was tested for its ability to support ATP hydrolysis by MinD. As showin in Figure 3.14, there was no evidence of ATP hydrolysis being stimulated beyond background levels. These results imply that the negative charge in the phospholipid headgroup is essential to support MinE-stimulated ATP-hydrolysis by ATP.

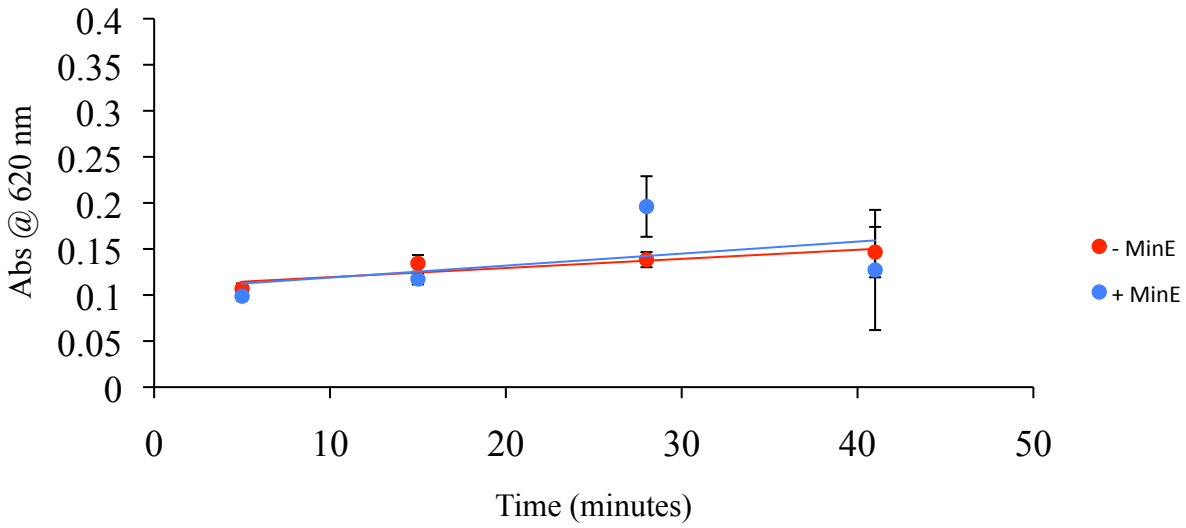

Figure 3.14: Representative initial rate profiles for MinE-stimulated MinD ATPase activity using DOPC phospholipids during late phase*. Reaction conditions as described in Figure 3.2 with the 0.5 mg/mL DOPC vesicles in place of DOPG and the + MinE reaction containing 3 µM MinE.*

3.9 The effect of lipid fluidity on MinD activity

Another characteristic of the membrane that may be important for MinD activity is that of membrane fluidity. To test this hypothesis, MinD kinetic profiles were acquired using POPG, an assymetric lipid containing one C18 acyl chain with a single unsaturation site, and one saturated C16 acyl chain, resulting in a lipid bilayer with a phase transition temperature significantly higher than that of DOPG with its two singly unsaturated C18 acyl chains (-2 ^{o}C versus -18 ^{o}C). Therefore the fluidity of the POPG membrane will be lower than that of DOPG, but still higher than that of *E. coli* lipid. As shown in Figure 3.15, when MinE-stimulated MinD activity was measured as a function of MinE concentration with POPG vesicles, maximal MinD ATPase activity was 15±2 (Pi nmol/mg MinD/min), which was approximately half that obtained with DOPG. In contrast, the apparent affinity ($K_{0.5}$) with POPG was the same as that obtained with DOPG. These results suggest that the fluidity of the bilayer is an important determinant for V_{max}, but not $K_{0.5}$.

To determine if the reduced mobility of the lipid phase also affects the presence of a distinct early phase in the MinD kinetic profile, a complete initial rate profile was acquired, with frequent sampling during the first five minutes of the reaction. As shown in Figure 3.16, linearity was maintained over the full length of the measurement, with no evidence of a distinct early phase. This suggests that the early faster phase observed with DOPG MinD ATPase activity cannot be supported by the less mobile POPG bilayer.

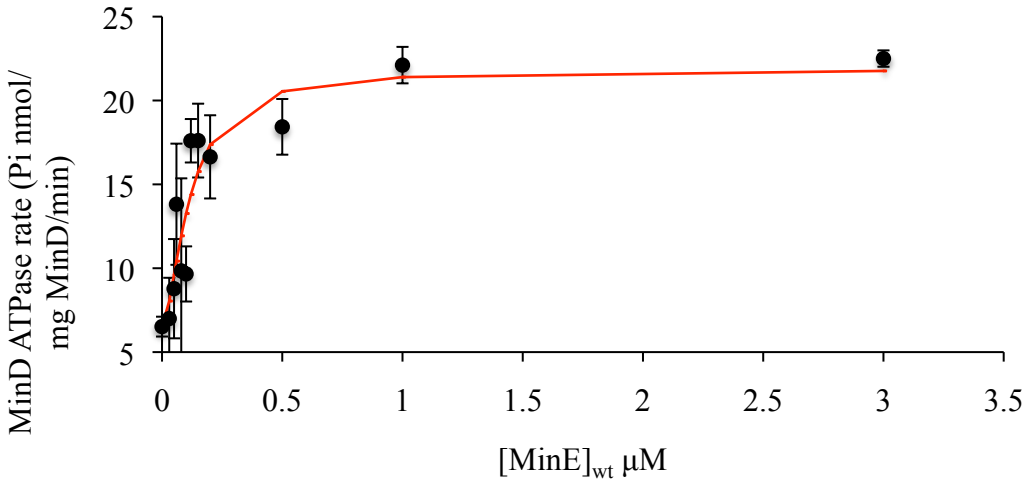

Figure 3.15: MinE-stimulated MinD ATPase activity with POPG. Rates were measured with aliquots taken between 5 and 41 minutes after initiation of the reaction. *The fit shown (red line) was obtained with V_{max} = 15±2, $K_{0.5}$ 0.11±0.02 mM and h = 1.60±0.04 by fitting the kinetic profile to the Hill equation.*

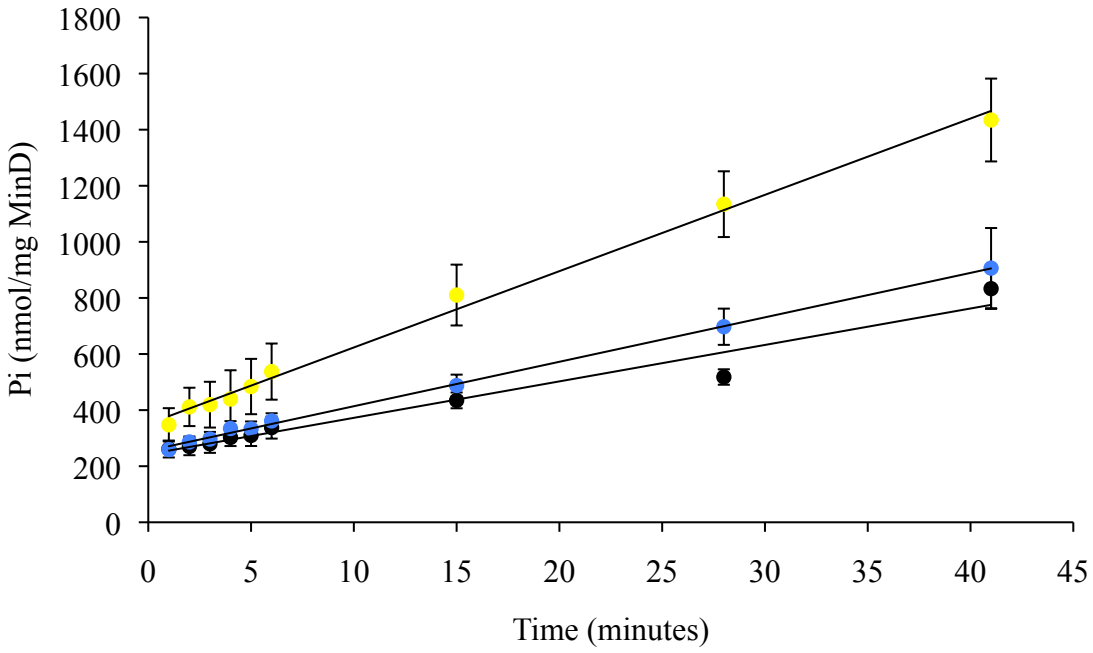

Figure 3.16: Initial rate profiles for MinE-stimulated MinD ATPase activity with POPG. *Reactions conditions are as described in Figure 3.2 with 0.5 mg/mL POPG vesicles used in place of DOPG, and 0 μM (black), 0.06 μM (blue) and 2.2 μM (yellow) MinE.*

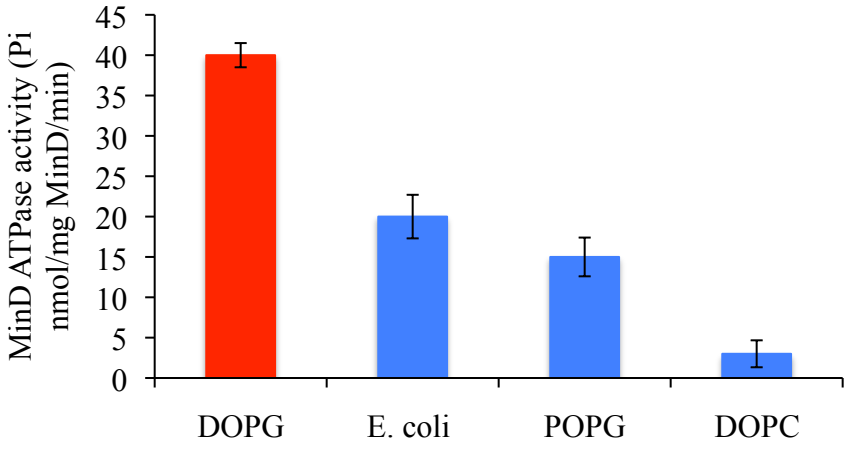

Figure 3.17: Summary of maximal MinD ATPase rates using different types of phospholipid (late phase measurements). *All reactions contained 2.7 μM MinD, 3 μM MinE and 0.5 mg/ml of lipid and 1 mM ATP. The only lipid that gave rise to distinct early and late phases was DOPG (red) with all others showing a single type of kinetic behavior over early and late regions of the rate profile (blue).*

Table 3.1: Summary of kinetic parameters obtained for MinE-stimulate MinD ATPase activity.

Lipid type	Phase	V_{max} (Pi nmol/mg MinD/min)	$K_{0.5}$ (μM)	Hill coefficient
DOPG	Early	244±29	0.45±0.12	2±0.07
	Late	37±2	0.11±0.02	2.9±0.3
E. coli	Late	20±3	0.020±0.004	2.5±0.2
POPG	Late	15±2	0.11±0.02	1.60±0.04

3.10 Optimization of MinD digestion by immobilized proteases

My results have shown the impact of membrane charge and fluidity on the rates of MinE-stimulated ATP hydrolysis by MinD. In addition, previous fluorescence imaging studies of Min proteins, both *in vivo* and *in vitro*, have demonstrated that the structure of the MinD/MinE polymer can be dramatically affected by changes in the composition of the lipid bilayer. These observations raise the possibility that the differences in kinetic parameters that I observed with the different membrane systems are caused by differences in the structure of the MinD polymer. However, the structure of the polymer under the conditions used to assay MinD activity has not been characterized. Moreover, there is no detailed structural information on the interactions between Min proteins that give rise to these nanoscale (*in vivo*) and mesoscale (*in vitro*) structures. Consequently, we are interested in developing a method that will allow us to characterize the interactions that occur in the MinD polymer in the same conditions as are used for our ATPase assay. An ability to correlate the functional measurement to a structural measurement would bring unique insights to the Min system, potentially allowing a mechanism to be uncovered for the growth and decay phases of the MinD polymer.

One method that can be used to obtain detailed information on the residues involved in polymerization is chemical modification. As described in the introduction, identification of modification sites requires that the sample undergoes proteolysis, and the peptide mixture be analyzed by MS. While this method has been used to characterize the structures of actin polymers (57), it has never been applied to the Min proteins. Consequently, it is necessary to develop a protocol that is tailored to the special features of MinD and its requirement for lipid membranes for polymer assembly.

The first aspect of the assay that was investigated was the identification of a protease that could effectively reduce the full-length MinD into a diverse population of peptides that could be easily analyzed by ESI-MS (~0.2– 4.5 kDa). The protease needed to be obtained in an immobilized form that would allow its rapid removal from the reaction after digestion.

The enzyme that was tested for this purpose was immobilized trypsin, since it is an inexpensive, robust and with a well defined substrate specificity. We used a cross-linked form of trypsin that is conjugated to cellulose resin, facilitating its straightforward removal. As demonstrated in Figure 3.18, when MinD was exposed to this immobilized trypsin for one minute, the band that corresponds to full length MinD (lane 1) disappeared after 1 minute of digestion with a new set of bands appearing with a molecular weight less than 24 kDa (lane 2). The preservation of a larger fragment of MinD suggested that a diverse pool of peptides could be produced under these reaction conditions.

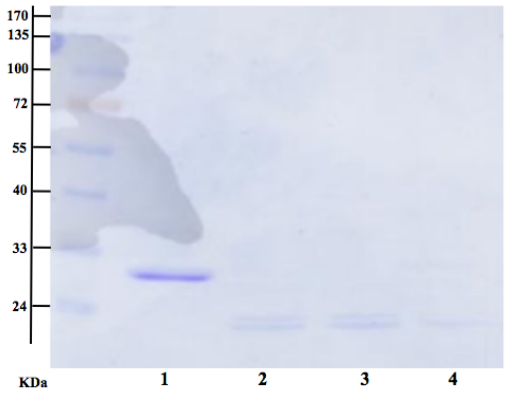

Figure 3.18: SDS-PAGE of MinD after digestion with immobilized trypsin*. 6 μM MinD in 50 mM ammonium bicarbonate pH 7.5 (lane 1) was digested by 300 units of immobilized trypsin for 1 (lane 2), 2 (lane 3) and 5 (lane 4) minutes.*

To determine if the trypsin digestion produced a diverse mixture of peptides suitable for our intended application, we performed MALDI-MS on the digestion product. Prior to digestion, MALDI-MS showed strong intensity at a m/z ratio of ~30,527 KDa, which is in good agreement with the expected MinD molecular weight (30,662 KDa). A shoulder peak was also observed at m/z ratio of 30707 KDa, likely due to a small population of MinD that has not had its N-terminal methionine post-translationally removed. In the sample prepared following the digestion by immobilized trypsin, these peaks were no longer visible, and instead a large number of new species appeared with m/z ratios of 4,500 and below (Fig. 3.20). Therefore the digestion conditions used for this sample seemed to be appropriate for the generation of a mixture of peptides with the desired mass range.

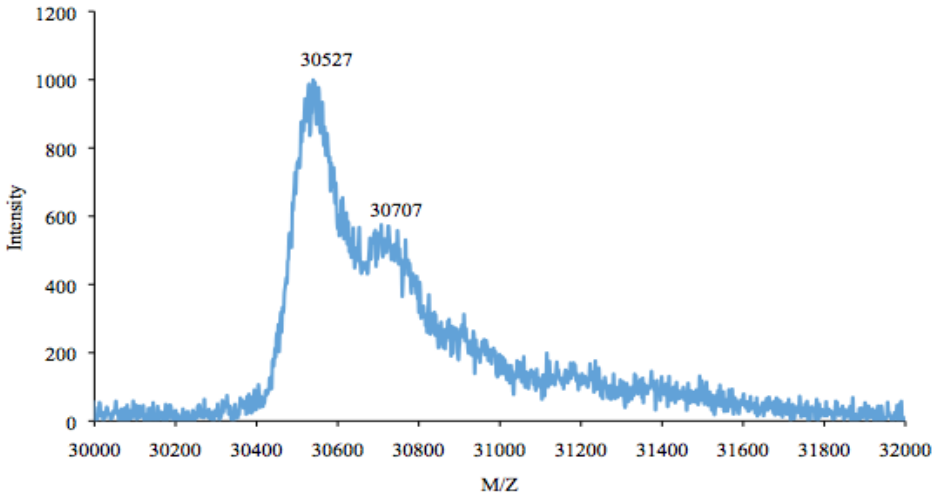

Figure 3.19: MALDI-MS profile of full length MinD. *6 µM MinD in 50 mM ammonium bicarbonate was mixed with sinapic acid (1:1, v/v) and 1 µL added to the MALDI plate and dried at room temperature.*

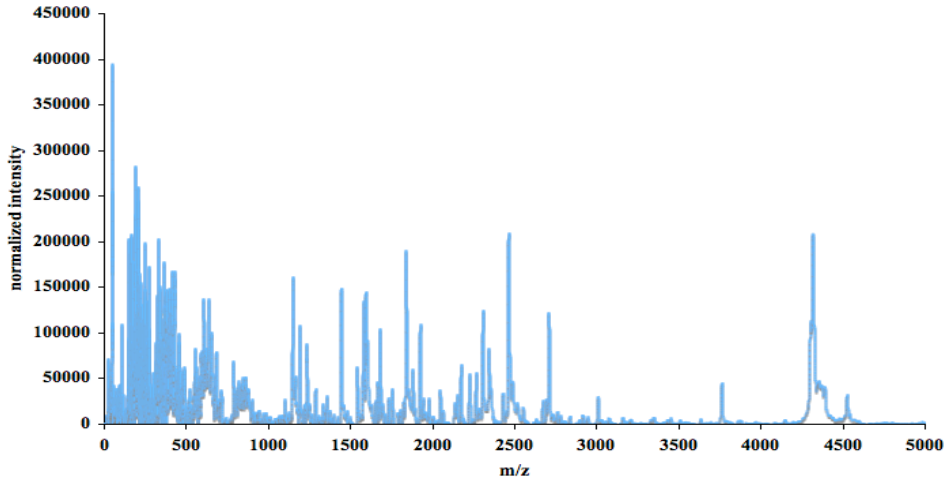

Figure 3.20: MALDI-MS spectrum of the peptide mixture produced by tryptic digest of MinD. *6 µM MinD in 50mM ammonium bicarbonate at pH 7 was treated with 60 units of immobilized trypsin for 5 minutes (6:1 (v:v) MinD:trypsin). A sample was removed from the resin and prepared for MALDI-MS as described in the previous figure legend.*

To identify the peptides produced by this digestion an LC-MS/MS experiment was performed by Prof. Jeff Smith (Department of Chemistry, Carleton University). LC MS/MS allowed some separation of the peptide mixture to be achieved by reverse-phase chromatography prior to the MS/MS. This instrument also afforded much higher accuracy in m/z ratio measurements compared to the ± 8 Da accuracy we obtained with

MALDI-MS. In addition, it was possible to identify peptides for ~23% of the MinD sequence (summarized in Table 3.2). The recovered peptides were mapped to the MinD structure and found to localize largely to surface α helices and buried β sheets (Fig. 3.21). This preliminary result is encouraging since additional recovery in a range of ~10-20% of the MinD sequence will likely be obtained by using longer gradients during the LC step to further reduce the complexity of the peptide mixture undergoing MS at any one time.

Table 3.2: Peptides produced from MinD-tryptic digest identified by LC –MS/MS.

Range	Sequence
1-11	MAKIIVVTSGK
4-11	IIVVTSGK
4-16	IIVVTSGKGGVGK
12-16	GGVGK
12-30	GGVGKTTTSASIATGLALR
31-33	GYK
34-54	TAVIDFDVGLRNLDLIIMGCER
45-54	NLDLIMGCER
79-92	NCENLFILPASQTR
93-99	DKDALTR
95-99	DALTR
100-112	EGVEKVMQELSGK
105-112	VMQELSGK
154-157	DSDR
177-183	EHLLITR
184-188	YSPER
189-192	VAK
247-252	LLGENR
247-255	LLGENREMR

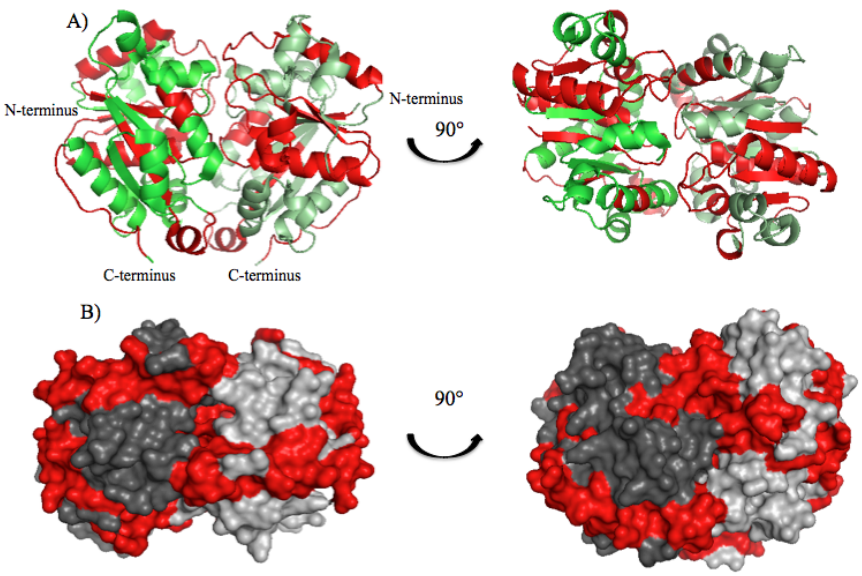

Figure 3.21: Origin of peptides produced by tryptic digestion mapped onto the structure of the MinD dimer. *Red regions of the MinD ribbon (A) and surface (B) structures correspond to peptides produced by tryptic-digestion of MinD. The surfaces of MinD corresponding to peptides not obtained from the digest are highlighted in two different shades of green (A) and grey (B) to differentiate the two subunits. The structure shown is the ATP-bound hydrolysis-deficient mutant of E. coli MinD with a 10-residue C-terminal truncation (Lutkenhaus 2011) (PDB:3Q9L) (35).*

3.11 Optimization of a MinD isolation protocol to follow the labeling reaction

In order to develop an assay to probe Min polymer structure it was necessary to find a protocol to isolate MinD from the chemical modification reaction mixture. Since previous studies (21, 25, 41) showed that MinD binds to lipid vesicles in the presence of ATP, we tested whether this could be used to isolate MinD once the labeling reaction was completed. For this purpose, vesicle sedimentation of lipid-bound MinD was tested in the presence of ATP and Mg^{2+} (41). However, as shown in Figure 3.22, centrifugation of the reaction mixture did not give rise to a reasonable yield for MinD in the lipid pellet, with only ~8% of the total protein localizing to this fraction. While it is possible that the use of an ultracentrifuge to access higher spinning speeds should help to improve this yield, previously work suggests that only ~15% yields could be anticipated for MinD (47). Moreover, the isolated MinD fraction would contain a significant amount of phospholipids that could interfere with downstream MS experiments. Consequently, we

decided to use nickel affinity chromatography as the post-labeling purification method, since this should also allow removal of phospholipids from the reaction mix. Feasibility studies with small-scale nickel affinity purification showed that yields of ~40% could be achieved (Fig. 3.23).

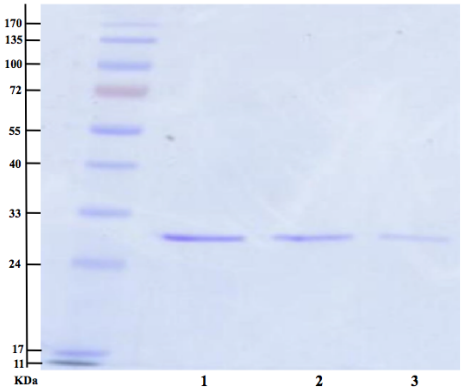

Figure 3.22: Example of MinD isolation using vesicle sedimentation. *2.7 µM MinD in exchange buffer pH 8.5, 5 mM $MgCl_2$, 0.5 mg/ml E. coli lipid (large vesicles ≥ 500 µm) was incubated with 1 mM ATP for 20 minutes. Reactions were centrifuged for 10 minutes at 16,000xg and pellets resuspended in 50 µl 50% ACN and 0.1% TFA to allow SDS-PAGE and MALDI analyses. The Coomassie stained SDS-PAGE is shown with untreated MinD (lane 1), the supernatant after centrifugation (lane 2) and the resuspended pellet (lane 3). Based on integrated band intensities the yield of MinD obtained in the pellet fraction is 8%.*

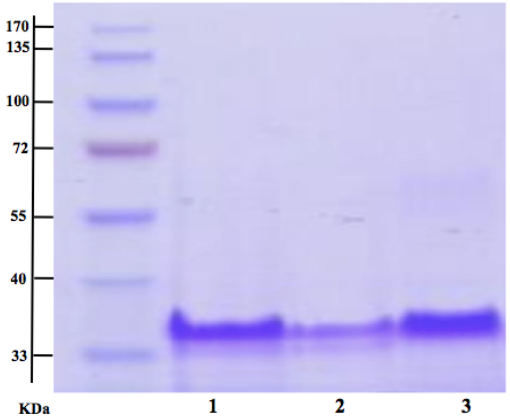

Figure 3.23: MinD isolation by nickel affinity chromatography. *6 µM MinD in 0.5 mL size exclusion buffer pH 8.5, 5 mM $MgCl_2$, 0.5 mg/ml DOPG lipid (multilamellar vesicles) was incubated with 1 mM ATP for 15 minutes. The reaction mixture was transferred to a column containing 150 µL of Ni-NTA resin, and MinD eluted with 200 µL 250 mM imidazole. Based on integrated band intensities, the yield of MinD obtained is 42%. Shown in the gel are samples taken from the MinD that was applied to the column (lane 1), a washing step (lane 2) and the eluted sample (lane 3).*

3.12 Optimization of the Fenton reaction for the covalent modification of solvent-exposed regions of MinD

The final aspect of the labeling assay that needed to be developed was the labeling reaction itself, which in our case would use hydroxyl radicals produced by the Fenton reaction. However, previous examples of covalent modification using the Fenton reaction required significant concentrations of EDTA to maintain the iron catalyst in solution, a reagent that is not very compatible with nickel affinity chromatography. Nonetheless, the resin that we were using could tolerate lower concentrations of EDTA (<1 mM), suggesting that it could be retained in the reaction so long as it was kept within this concentration range. Since previous Fenton-based labeling reactions had used EDTA concentrations of 25 mM, it was necessary to modify the reaction conditions to reduce the amount of EDTA.

For this series of experiments, a smaller water-soluble protein was used as a model to help simplify the analysis, namely the 8 kDa cytoplasmic domain from the *E. coli* GlpG rhomboid protein (RCD). Although MALDI-MS of the purified RCD showed that it had undergone some proteolytic degradation, giving rise to a mix of degradation products (Fig. 3.24), we chose to continue with this sample since it was highly soluble with a low molecular weight that would easily show the effects of oxidation in the mass spectrum. Since we needed to reduce the concentration of EDTA in our reaction we also decreased the concentration of the Fenton solution that provides the iron needed to catalyze radical formation (ferrous ammonium persulfate). As shown in Figure 3.24, when 4 mM Fenton solution was used with 10 mM EDTA, there was an upward shift in m/z ratios for all peaks in the spectrum, as would be expected for a sample that has undergone oxidation. Moreover, when these concentrations were reduced 10-fold (both EDTA and Fenton solution), a similar shift was also observed, although smaller in magnitude than that seen with the higher concentrations. This suggested that it should be possible to obtain oxidized samples at EDTA concentrations that should be compatible with nickel affinity chromatography.

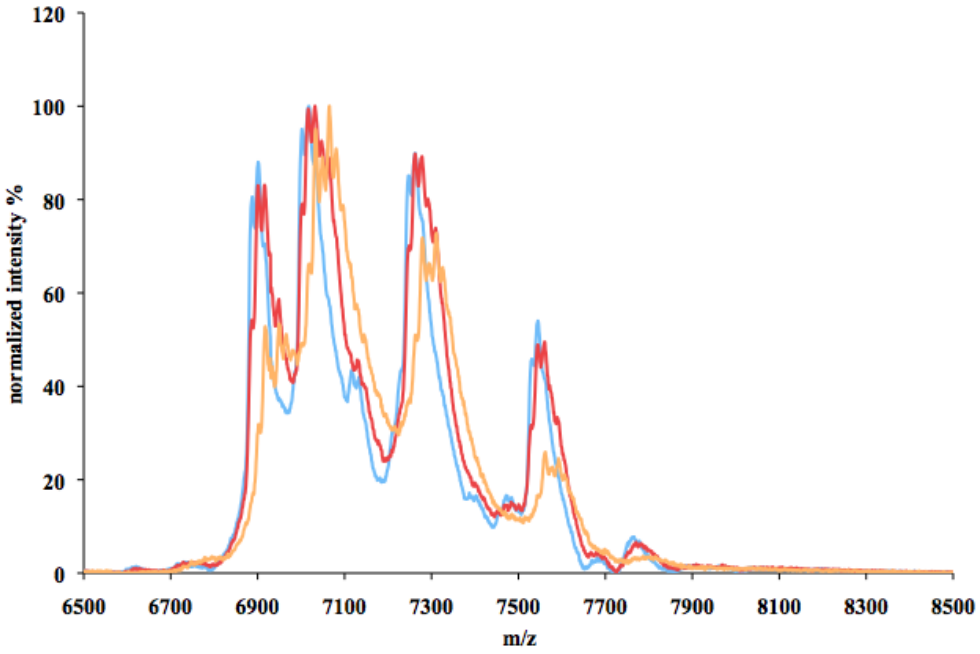

Figure 3.24: MALDI-MS spectra of RCD. *6 μM RCD in size exclusion buffer pH 8.5 (blue) was incubated with a 0.4 mM Fenton solution (ferrous ammonium persulfate), 1 mM EDTA (red) or with a 10-fold higher concentration of these two reagents (orange), along with 0.3% H_2O_2 for 5 minutes. Samples were removed immediately and mixed with MALDI matrix and allowed to dry for less than a minute before being analyzed by MALDI-MS.*

In order to determine the minimum hydrogen peroxide levels required to promote oxidation, different concentrations of hydrogen peroxide were also tested using lower concentrations of EDTA and Fenton solutions. As shown in Figure 3.25, when 0.5 mM EDTA and 0.5 mM Fenton solutions were incubated with increasing concentrations of hydrogen peroxide, the shift in m/z ratios increased, suggesting more extensive oxidation at these higher concentrations. However, since the increase in mass at higher peroxide concentrations could come from oxidation of a wide range of amino acids, we decided to stay with lower concentrations of peroxide to simplify analysis. Under these conditions, only those side chains that are more susceptible to labeling, such as methionine, should be labeled, although this will need to be confirmed by MS in the future.

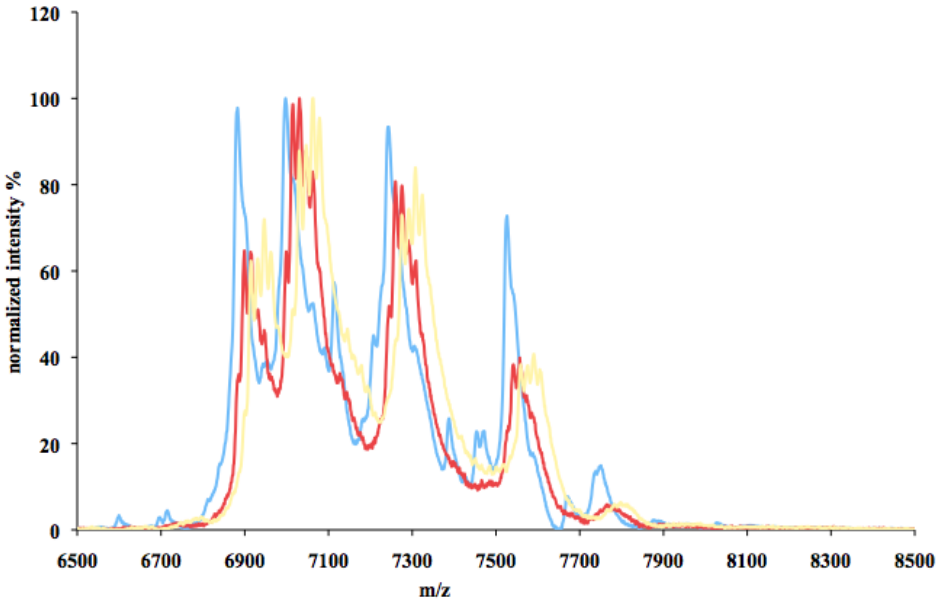

Figure 3. 25: MALDI MS of RCD (blue) incubated for three minutes with 0.5 mM of Fenton solution, 0.5 mM EDTA, and 0.3% (red), or 1.2% (yellow) H_2O_2.

During the optimization process, SDS-PAGE was also used to evaluate the effect of oxidation on the MinD sample. As shown in Figure 3.26, the band corresponding to oxidized MinD was significantly reduced in intensity compared to non-oxidized samples. This seemed to be a specific effect of the oxidation reaction, since incubation with one or more reaction component did not produce this extent of intensity loss. A smaller amount of intensity loss was observed in the presence of Fenton solution together with hydrogen peroxide, likely reflecting a small amount of oxidation that can be carried out even in the absence of EDTA. Nonetheless, when EDTA was included in this mixture, its ability to keep the iron in solution under the reaction conditions used seems to greatly facilitate oxidation, as expected (86). While the cause of the intensity reduction is not clear, with no evidence of aggregation in gel wells or in the solution, it is possible that the oxidized sample has a reduced tendency to bind the Coomassie stain. In fact, it is known that proteins that are subject to reactions with hydroxyl radicals show a decrease in isoelectric point (88). Given that the Coomassie dye binds to positively charged residues (89), it is possible that this loss of positive charge at least partly explains the loss in band intensity on these gels.

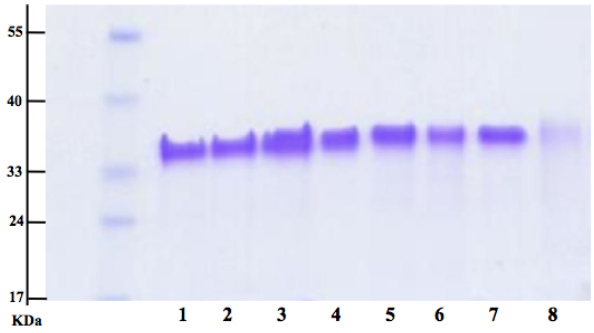

Figure 3.26: SDS-PAGE analysis of oxidized MinD. Total volume was 100 µL, with 6 µM MinD in all reactions*. MinD with all reagents required for the oxidation reaction (500 µM of ferrous ammonium presulfate (Fenton solution), 500 µM EDTA and 0.3 % H_2O_2) is shown in lane 8. Control lanes contained MinD alone (Lane 1), with EDTA (lane 2), Fenton solution (lane 3), EDTA and Fenton solution (lane 4), H_2O_2 (lane 5), Fenton solution and H_2O_2 (lane 6), or EDTA and H_2O_2 (lane 7).*

3.13 Application of oxidation protocol to MinD

To evaluate the efficacy of the oxidation protocol for MinD when bound to lipids, MinD was mixed with ATP and vesicles made from DOPG. This mixture was then incubated with 0.3% H_2O_2 for 3 minutes in presence of 0.5 mM Fenton solution and 0.5 mM EDTA. The reaction mixture was then subjected to nickel affinity chromatography followed by a 3 minute exposure to 60 units of immobilized trypsin. A parallel sample was also prepared as a control that went through all procedures except incubation with oxidation reagents. As shown in Figure 3.27, MinD was successfully isolated by nickel chromatography after oxidation. Although some sample was lost in the column wash, a significant proportion was retained that was sufficient for subsequent manipulations. As observed previously, the intensity of the MinD band after purification was significantly lower for the oxidized sample. After exposure to trypsin this band was no longer present, and replaced by several lower molecular weight species, although these products of digestion were of very low intensity in the oxidized sample likely due to the reduced staining intensity of oxidized samples. Unfortunately, limitations in our access to LC-MS/MS instrument time did not allow samples of oxidized MinD to be run, with only the control sample being analyzed. Nonetheless, further optimization of the digestion and LC-MS/MS protocols should allow larger sequence coverage to be achieved in the future.

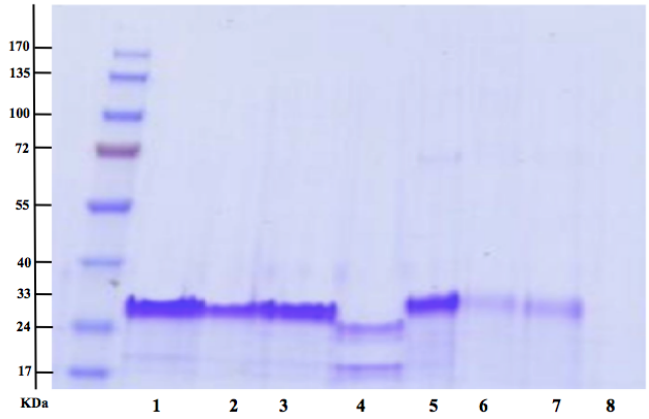

Figure 3.27: SDS-PAGE of samples taken at various stages of the MinD oxidation protocol. *6 µM MinD with 0.5 mg/ml DOPG vesicles, 5 mM $MgCl_2$ and 1 mM ATP was incubated with 0.5 mM EDTA, 0.5 mM Fenton solution and 0.3% H_2O_2 for 5 minutes. Reactions were then transferred to a micro-column containing 150 µL Ni-resin. The resin was washed with 50 µL of 50 mM Tris pH 8 (3 times) and then eluted by 100 µL 250 mM imidazole. Purified MinD was incubated with 60 units of trypsin for 5 minutes and peptides were concentrated and desalted using a C_4 ziptip. Final peptide mixtures were eluted in 50% methanol and 1% formic acid. Lanes 1-4 represent control and 5-8 oxidized samples. Lane 1 (5) shows the MinD sample, 2 (6) is a fraction from the wash step in the affinity purification, 3 (7) is eluted MinD, and 4 (8) is the sample following the MinD-tryptic digest.*

Chapter 4: Discussion

4.1 MinD kinetic assay

The interaction between MinD and the surface of the bacterial inner membrane is a critical step in the regulation of bacterial cell division by the Min system. Not only is this binding event required to bring the MinC inhibitor of cell division to the membrane where it can interact with FtsZ, but it is a fundamental requirement for MinD-catalyzed ATP hydrolysis and formation of dynamic higher order structures. As described in the Introduction, these interactions with the membrane can be altered by the physical properties of the lipid bilayer. Specifically, MinD has been shown to preferentially interact with membranes comprised of lipids having anionic headgroups and lower melting temperatures (47). Meanwhile MinD also induces changes in membrane properties upon binding, increasing the order and decreasing mobility of the constituent lipids (48). Prior to the work performed in this thesis, the influence of these physical properties of the membrane on ATPase activity of MinD had not been studied. However, by monitoring the MinE-stimulated MinD ATPase activity as a function of MinE concentration, we were able to obtain kinetic parameters that could be compared from one lipid system to the next.

One of the kinetic parameters shown to depend on lipid type was the maximal rate of MinD-catalyzed ATP hydrolysis (V_{max}), a constant that is related to the MinD catalytic constant k_{cat}. In the steady state model of enzyme kinetics, k_{cat} is a function of the rate constants of all steps that do not depend on the concentration of ligand (k_i), which in our analysis is MinE. If all those steps were first order reactions then:

$$\frac{1}{k_{cat}} = \sum_i \frac{1}{k_i}$$

with more complicated expressions being required to incorporate any higher order steps in the reaction sequence (90). According to this relationship, the magnitude of k_{cat} will be dominated by the speed of the rate-determining step, particularly if it is much slower than

the other steps in the reaction. Hence, to gain better insight into the physical meaning of our measurements, it will be useful to identify the steps involved in the reaction cycle, and characterize their associated rates.

In the case of MinD, the reaction cycle likely involves a number of kinetically resolvable steps involving membrane, ATP and protein binding events. An example of a kinetic reaction mechanism that could be proposed that incorporates these steps is:

$$2D + 2\,ATP \underset{k_{-1}}{\overset{k_1}{\rightleftharpoons}} \mathbf{DD} + membrane \underset{k_{-2}}{\overset{k_2}{\rightleftharpoons}} \mathbf{DD^*} + E \underset{k_{-3}}{\overset{k_3}{\rightleftharpoons}} \mathbf{DD^*}E \xrightarrow{k_4} \underline{DD^*E + 2\,P_i \xrightarrow{k_5} 2\,D + E}$$

where D is the ADP-bound, and **D** is the ATP-bound state of MinD, with the monomeric state being represented by a single D, the dimeric state by DD, and the membrane-bound state denoted with the asterisk. In this scheme the MinE dimer, shown as E, only binds to a single site on the MinD dimer, following a recently proposed model based on the results obtained with mutant MinD heterodimers with one of the two MinE-binding sites being inactivated (91).

It should be noted that the reaction scheme outlined above is just one of a large number of possible kinetic mechanisms, with some steps being either potentially broken down further, or combined in a concerted reaction. For example, the underlined portion of the kinetic reaction could be replaced by a single step where ATP hydrolysis is coupled to dissociation of the MinD dimer (i.e. **DD***E $\rightarrow$ 2D + E). An additional factor that has also not been incorporated into the proposed scheme is potential interactions that may occur between MinD dimers. In fact, not only is it possible that MinD forms oligomers with different catalytic efficiencies, but the oligomer may be the only state that can hydrolyze ATP. Consequently, the unknown number and type of steps that are needed to describe the kinetic reaction mechanism of the Min cycle, along with the unknown role of the MinD oligomer in the reaction cycle, make it impossible to definitively say what the slowest step might be without more information on the rates and players involved for each of these individual steps.

Although it is not yet possible to identify the rate determining step in the catalytic cycle, we have made the assumption in previous work that our measurements of MinD activity reflect the rate of ATP hydrolysis (31); in other words, that the ATP hydrolysis step is the rate-determining step in this reaction sequence. One of the justifications for this assumption was provided by the correlation that has been observed between MinD-catalyzed ATP hydrolysis rates and the length of the MinD oscillation cycle. Specifically, mutations of K19 in MinE that give rise to lower rates of ATP hydrolysis tend to increase the amount of time it takes for the Min polymer to grow and decay at each side of the cell (30). However, the effect of this mutation on kinetic parameters that can be used in comparative studies (i.e. V_{max}, $K_{0.5}$ and h) has not been evaluated. Since previous results suggest that V_{max} is generally not affected by mutations in MinE (31), the previously reported association between oscillation rates and MinD ATPase activity is more likely caused by a decrease in the affinity of MinE for MinD, as would be predicted by the MinDE structure (10).

To date, some of the best evidence to support a link between ATP hydrolysis rates and oscillation is provided by the MinD mutant D40A. This residue is involved in activating the water molecule required for nucleophilic attack of the ATP γ phosphate, with its mutation generating a catalytically deficient enzyme that binds ATP, self associates, localizes to the cell membrane and binds to MinE, but does not undergo oscillation (35). This mutant was only approximately 10-fold slower in its MinE-stimulated ATP hydrolysis rate compared to that of the wild-type enzyme (91). Future kinetic experiments on this mutant will be required to confirm that the only effect of this mutation is to reduce the magnitude of V_{max} without altering the apparent affinity for MinE, however, this result suggests that ATP hydrolysis serves as the molecular switch that controls the timing of Min protein oscillation.

Additional evidence that ATP hydrolysis is rate-limiting can also be found in previous studies that characterized the MinD-coated lipid tubules formed from vesicles in the presence of ATP (41). Light scattering of this reaction mixture was found to decrease upon addition of MinE to these tubules, corresponding to the dissociation of these

structures as observed by electron microscopy. The ATPase activity of MinD was also studied under these same conditions. Based on the data shown (41), we can estimate the maximal activity under these conditions, and find it to be approximately 10 nmol/min/mg MinD, which corresponds to a k_{cat} of 5×10^{-3} s^{-1}, and hence a turnover time of ~200 s. This corresponds very closely to the amount of time it takes for the light scattering of these samples to decrease to the new steady-state levels. Since light scattering is monitoring MinE-stimulated lipid tubule disassembly, these results suggest that ATP hydrolysis does not occur faster than tubule-disruption, supporting the hypothesis that ATP hydrolysis is the rate-limiting step.

In spite of the evidence that ATPase rates can be correlated with oscillation rates, it should be noted that similar studies on a mutant of Ng MinD could be considered to contradict this idea (10). Specifically, an N-terminal truncation of three amino acids in Ng MinD gave rise to a decreased rate of MinE-stimulated activity, but a faster rate of oscillation in *E. coli* relative to that of wild-type Ng MinD. However, the effect of this truncation appears to be multifaceted, since dimerization and MinE binding were both greatly reduced as measured in bacterial two-hybrid assays, and most of this mutant actually localized to the cytoplasm. Although it is not possible to know which of these defects gave rise to the more rapid oscillation rate, these results raise questions regarding the validity of drawing a direct relationship between ATP hydrolysis rates and the length of the Min protein oscillation cycle.

In order to more conclusively demonstrate that ATP hydrolysis is the rate-determining step, and to draw a link to Min protein oscillation, it will be necessary to do additional experiments in the future to monitor the rates of the various steps involved in the Min cycle. For example, stopped-flow experiments could be done to monitor the rate of phosphate production in the very early stages of the reaction to measure the rate of a single turnover, before steady-state conditions are reached (92). If a higher rate of phosphate production was obtained in this measurement, then this would suggest that ATP hydrolysis is not the rate determining step, but rather, some downstream event such as dissociation of MinD from the membrane, or nucleotide exchange. A similar approach

could also be used to measure the rate of MinD dissociation by introducing a single Trp into the MinD MTS, since it has been shown that the fluorescence of this Trp would increase upon membrane binding (23). Stopped-flow experiments could be done starting with pre-assembled MinD-coated lipid tubules, and the rate of Trp fluorescence intensity decrease upon introduction of MinE could be measured. If this rate were the same as the rate of phosphate production, this would be good evidence that Min polymer dissociation is controlled by ATP hydrolysis.

One other part of the cycle that should also be considered as a potential control point is MinD nucleotide exchange, particularly since this has been shown to be the slowest step for small GTPase enzymes such as Ras (93). A slow nucleotide exchange rate also holds the attraction that it would provide time for monomeric ADP-bound MinD to diffuse to the other cell pole after being released from the membrane during the oscillation cycle. For this reason it would be interesting to measure the rate of nucleotide exchange for MinD. If this rate of exchange is relatively slow then it may be possible to use solution NMR of MinD to measure this rate in the future as has been done for the Ras proteins (93). This involves monitoring time-dependent changes in NMR spectra of the target protein after addition of the nucleotide to be exchanged. In the case of MinD it would be necessary to remove the C-terminal membrane targeting sequence to improve its solubility, a modification that does not alter its propensity to bind ATP and dimerize (21). If successful, this data would provide a more accurate view of the diffusion properties of MinD during the oscillation cycle, and would also help to identify the rate-determining step in the reaction.

One other aspect of the Min protein reaction cycle that further complicates interpretation of the MinD kinetic parameters is the fact that it is still not known when in the oscillation cycle MinD ATP hydrolysis really occurs. For instance, the basic model suggests that ATP hydrolysis occurs as soon as MinE binds to membrane-bound MinD. However, studies of fluorescently-labeled Min protein on supported membranes suggest that MinD and MinE can cycle on and off the membrane more rapidly than ATP is hydrolyzed. Specifically, residence times measured for MinD on the membrane surface

range from ~4 – 8 s, with more densely covered membrane surfaces giving rise to longer residence times. Converting the ATP hydrolysis rates we measured on *E. coli* membranes into units of k_{cat} gives 2 x 10^{-2} s^{-1}, corresponding to a MinD turnover time of ~50 s. This very slow reaction time for MinD is difficult to reconcile with the short membrane residence times measured on planar membranes, and raises the possibility that ATP hydrolysis does not drive membrane dissociation for all states of MinD. Instead, it may be possible that ATP hydrolysis is only required to push oligomeric MinD off the membrane, with dimeric MinD being free to dissociate from the membrane in its ATP-bound state. However, it should be noted that ATP hydrolysis rates measured in bulk solution may not accurately mirror those occurring on the supported lipid bilayers *in vitro*, and that ATP hydrolysis of MinD bound to these planar membranes could be as fast as, or even faster than, the MinD dissociation from the membrane. To resolve this issue in the future it will be useful to measure the rate of phosphate production in the same system that is used for those planar bilayer-imaging studies to determine if there are any differences from the rates we measure in bulk solution.

4.2 The role of the lipid bilayer in the MinD ATPase cycle

i) Membrane charge and fluidity on MinD ATPase activity

Most of the studies on MinD ATPase activity performed in our lab have used the anionic lipid DOPG, in part due to the ease of handling these lipids with its low gel to fluid phase transition temperature. However, the results from my thesis show that the rates of MinD-catalyzed ATP hydrolysis are actually faster on this lipid compared to that that on the more physiologically relevant *E. coli* lipid extract. The ~50% lower maximal activity obtained on *E. coli* lipids could be due to the difference in affinity of the MinD-membrane interaction, since MinD binds DOPG membranes with a more than 3-fold greater affinity than those made from *E. coli* lipid extracts. However, it is interesting that no ATPase activity was detected in our assay when membranes comprised of zwitterionic lipids was used, particularly since vesicle sedimentation studies suggest that the affinity is only two times lower than that for *E. coli* lipids (47). This suggests that that negative

charge on the membrane surface is required to promote a catalytically active state in MinD.

In addition to the effect of membrane charge on MinD activity, my results have also shown that membrane fluidity could influence the MinD-membrane interaction. This may also reflect differences in membrane binding affinities, since vesicle sedimentation assays with cardiolipin (CL) showed stronger binding when its alkyl chain composition gave rise to lower phase transition temperatures (47). This suggests that MinD has a preference to bind to more dynamic fluid membrane phases. In my experiments, lower maximal ATPase activity was observed when a PG lipid with a higher phase transition temperature was used. Since previous results suggest that MinD will have a reduced tendency to bind these less fluid membranes (47), it appears that the maximal activity depends, at least to some extent, on the affinity of the MinD-membrane interaction.

ii) Implications of the fast ATP hydrolysis phase on DOPG

Introduction of a heat-inactivating step in the MinD ATPase assay made it possible to monitor the MinD ATP hydrolysis reaction within ~1 minute of its start, allowing the detection of a faster phase over the first few minutes of the reaction on DOPG. This early phase of MinD ATPase activity showed a maximal rate that was 6-fold faster than that obtained when the later phase of the reaction was sampled, as had been done in all previous studies in the Goto lab (31). This translates into a k_{cat} measurement of 0.13 s^{-1}, corresponding to a turnover time of ~ 8 s, which is similar to the residence times observed for MinD on planar lipid bilayers (4.6 to 8.7 s). These early-phase measurements demonstrate that it is possible for MinD-catalyzed ATP hydrolysis to occur on a timescale that is compatible with the membrane residence times observed on planar bilayers although we do not yet understand the conditions that give rise to this faster rate.

Features of the early phase, including the larger amount of MinE required to reach half-maximal activity, and the higher V_{max}, are all consistent with a scenario where the

number of accessible MinE-binding sites changes over the course of the reaction on DOPG. According to this idea, the structure of the polymer and/or the extent of polymerization may differ in the initial stages of the reaction to give rise to more MinE-binding sites, and hence a larger measured activity due to the increased numbers of MinD active sites that can be stimulated to catalyze ATP hydrolysis. At a later stage of the reaction a steady-state structure of the polymer with a reduced number of MinE-binding sites would then dominate. Consistent with this idea is the fact that the late-phase measurement on DOPG reaches maximal activity at MinE to MinD ratios that are much less than 1:1 (Fig. 3.3). In fact, this ratio is approximately 0.1:1, suggesting that in the late phase not all MinD is available for MinE binding, even in its most active state. In contrast, maximal activation of MinD by MinE occurs at much higher MinE:MinD ratios, appearing to require a ratio of ~1:1 for saturation. The fact that V_{max} is also higher for early-phase measurements also suggests that more MinD active sites are able to hydrolyze ATP under these conditions. The increase in the hill coefficient that occurs at later stages of the reaction is also consistent with a change in the oligomer structure relative to the early phases of the reaction, with a larger number and/or more tightly linked MinE binding sites in the late phase polymer structure.

Support for this idea that MinE can not bind to all MinD subunits in the polymer has also been provided by a number of other studies. For example, fluorescence studies with Min proteins on planar bilayers under flow conditions that maintain a constant concentration of Min proteins in the aqueous phase show that MinE localizes to the edges of various types of polymers formed by MinD (54). Electron microscopy of MinD polymers also showed directional dissociation of the MinD polymer upon addition of MinE, suggesting that MinE only binds to one end of the polymer (41). More relevant to our *in vitro* ATPase measurements are fluorescence imaging studies on planar bilayers in isolated (i.e. non-flow) systems, giving rise to waves of MinD that move across the surface as described in Section 1.5. In subsequent studies fluorescence intensities in these systems were quantitated, showing that MinD accumulates on the membrane more rapidly than MinE accumulates on the MinD polymer as described in Section 1.5.

One consequence of a MinD polymer model where not all MinD can undergo MinE-stimulated ATPase activity is that the calculation for k_{cat} could be changed to focus on the part of population that can bind to MinE. Specifically, if we assume that only ~10% of MinD in this reaction was actually available for activation, the calculation of k_{cat} would use the concentration of activatable MinD (~0.2 μM), instead of the total concentration of MinD (2.7 μM). This gives a turnover time of ~4 s for this population, a timescale that once again becomes more compatible with measured membrane residence times on planar bilayers.

Although we have suggested that the MinD polymer contains a significant population that is not activated by MinE, it is also possible that ATP hydrolysis at multiple sites can be stimulated by MinE interactions at a single site. This latter scenario was investigated in a recent study measuring the activity of a MinD mutant that could not bind MinE, after it was mixed with wild-type MinD (91). The rate of MinE-stimulated ATP hydrolysis was found to be the same for a 1:1 mutant:wild-type mixture as the rate from the same amount of MinD that was 100% wild-type. The same rate was also observed when the mixture was 2:1 mutant:wild-type, suggesting that ATP hydrolysis occurs at a maximum of two sites for every single MinE-binding event. This implies that only a small part of the 1:10 MinE:MinD ratio required for maximal activation can be accounted for by multiple ATP hydrolysis events per MinE-binding event, which predicts a 1:2 ratio of MinE:MinD for maximal stimulation. Whether different regions of the MinD polymer will have different tendencies to bind to and/or be activated by MinE is a question that will require more information on the molecular nature of MinD interactions in the polymeric state, a goal we hope to achieve in the future.

4.3 Development of protocols to study MinD polymerization

One of the most significant gaps in our understanding of the Min system, highlighted by some the results in this thesis, is the molecular nature of the dynamic polymeric structures formed by Min proteins *in vivo* and *in vitro*. However, structural studies of these higher order polymers is challenging, and requires that new methods be

applied. In my thesis I have initiated the development of a protocol to identify residues in MinD involved in these higher-order interactions through the use of covalent labeling.

One of the steps in the method that we would like to improve in the future is the level of sequence coverage in the LC-MS/MS analysis. While no opportunity was available at the time of these trials to engage in optimization of the analysis, in the future we will be looking at methods that can improve the yields of digested peptides. For example, the high concentrations of imidazole that was used to elute MinD from the nickel affinity resin prior to digestion gave rise to a peptide mixture in a buffer that was not suitable for direct injection to the LC-MS/MS. Although it is straightforward to remove this salt using reverse-phase microscale batch chromatography (e.g. ZipTips) before LC-MS/MS analysis, the yields from this purification step may be low, and will depend on the physical characteristics of each peptide in the mixture. In the future we will explore alternative methods for elution from the nickel affinity resin. For example, acidification of buffer pH will promote elution by protonation of the histidine residues required for nickel coordination. Conveniently, if this condition is not compatible with subsequent digestion, then it is straightforward to raise the pH of the solution to return it to appropriate levels. In addition, the use of longer gradients during the LC step, combined with the use of larger amounts of peptide mixture should all help to increase the sequence coverage from the 23% coverage that we obtained in our first experiments.

Among the 19 peptides that were detected in our preliminary trial of unlabeled MinD, only three contained the most susceptible amino acid to oxidation; namely methionine. Moreover, only one of these Met-containing peptides is located on the surface of the MinD dimer structure. However, to increase our ability to probe wide surface area of MinD, we plan to use oxidation conditions that will modify more than just the methionine site. While we have not yet had the opportunity to analyze by LC-MS/MS any of the sample that we have subjected to oxidation, the appearance of an increasing array and number of higher molecular weight species upon exposure to higher concentrations of peroxide (Fig. 3.25) suggests that extensive oxidation can be achieved at multiple sites.

Once fully optimized, the covalent labeling approach has the potential to help identify changes in Min polymer structure under different assay conditions. However, in the event that this assay cannot be fully developed for this purpose, it should be possible to use alternate approaches to obtain this information. For example, identification of conserved residues on the surface of the MinD dimer structure that are not required for MinE or MinC binding may provide some clues into a potential role for polymerization. As shown in Figure 4.1, there are several surface exposed residues on the MinD dimer structure that are conserved across species, and could be targeted for mutagenesis. For example, MinD residues R54, R55, K76, K78 together form a well-conserved positively charged patch on the surface of the MinD dimer, and could be targeted for mutagenesis in the future. The ability of these mutants to undergo polymerization could be evaluated as has previously been done for wild-type MinD; for example by electron microscopy (41) or dynamic light scattering (41). The kinetic parameters of these mutants may also reveal changes in MinE binding cooperativity, or even maximal activity levels, data that would help to clarify the role of polymerization in the Min protein cycle. Ultimately, those mutants showing altered polymerization *in vitro* would need to be functionally evaluated *in vivo*, using established methods (10, 19, 40).

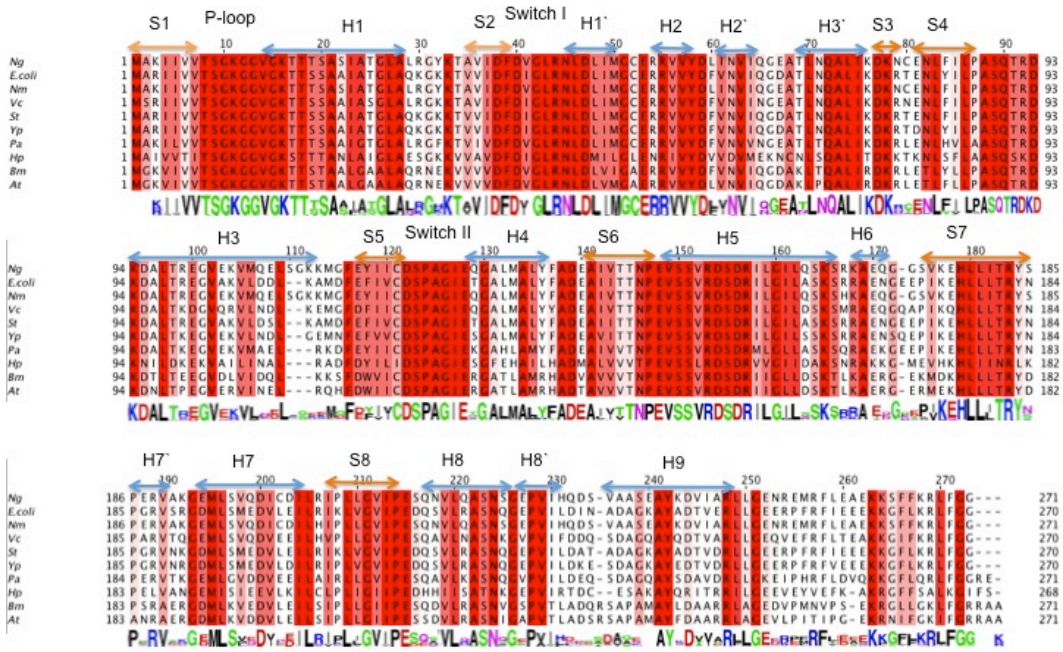

Figure 4.1: Amino acid sequence alignment for MinD from gram negative bacteria. *Sequence alignment was preformed with ClustalW2 (11) and sequence coloring of the alignment was done using Jalview (12). Red regions correspond to identical residues, and light red regions show homologous residues. Graphical presentation underneath MinD sequence aligments represents conserved MinD amino acids generated by Weblogo (94, 95). MinD sequences from 10 species of gram negative bacteria are shown, namely; Neisseria gonorrhoeae (Ng), Escherichia coli (E. coli), Neisseria meningitides (Nm), Vibrio Cholerae (Vc), Salmonella enterica serovar Typhimurium (St), Yersinia pestis (Yp), Pseudomonas aeruginosa (Pa), Helicobacter pylori (Hp), Brucella melitensis (Bm), Agrobacterium tumefaciens (At).*

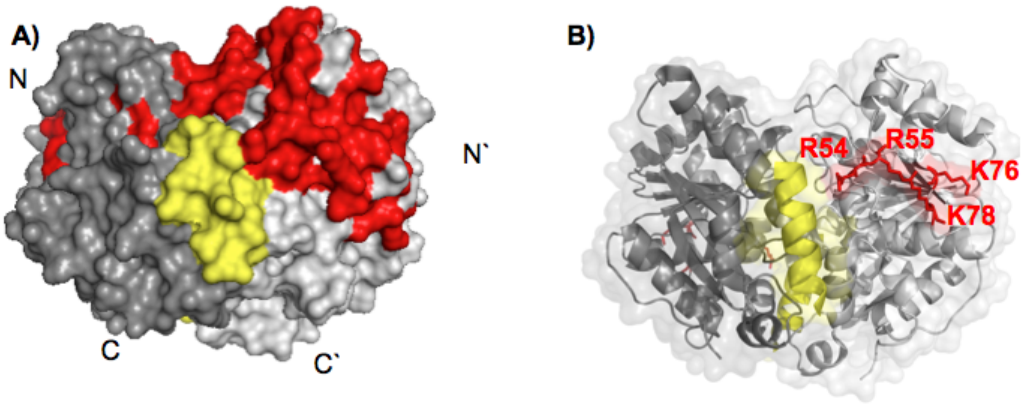

Figure 4.2: Surface of the MinD-MinE (residues 12-31) structure highlighting regions corresponding to conserved surface exposed residues*. A) MinD subunits are shown in dark and light grey, with surface-exposed conserved residues color coded in red, and the MinE peptide in yellow. B) Conserved positively charged MinD residues located on surface of the MinD dimer. (PDB accession number:3R9I, with same orientation as in Figure 1.3).*

4.4 Concluding remarks

The ultimate goal of the work of this thesis, together with other research going on in the Goto lab, is to understand how interactions between Min proteins, and between MinD and the membrane, contribute to the regulation of bacterial cell division by Min proteins. I have focused on the role of the membrane in regulating rates of ATP hydrolysis, and how different properties can modulate this activity. I have demonstrated that membrane charge is a requirement for MinD activation, and that membrane fluidity modulates the rate of MinD ATP hydrolysis. These results suggest a potential mechanism for the different dynamic phases observed for Min protein localization *in vivo* since the lipids are not uniformly distributed along the bacterial membrane (96-98). In addition, this may provide an explanation for why MinD binds and polymerizes at the cell pole rather than any other location since MinD should prefer to bind to regions of the membrane with higher concentrations of fluid anionic lipids. However, in the future, more work will be required to identify the point in the Min cycle when ATP hydrolysis occurs, and the molecular nature of the polymeric species that arise during oscillation.

Better understanding of Min oscillation at the molecular level will not only help identify susceptible points for inhibition of this process for the development of new antimicrobials, but will also provide insight into general mechanisms of dynamic pattern formation that is the basis of so many fundamental processes in life.

REFRENCES

1. Woldringh CL, Mulder E, Huls PG, & Vischer N (1991) Toporegulation of bacterial division according to the nucleoid occlusion model. *Microbiology* 142:309-320.

2. De Boer PAJ, Crossley RE, & Rothfield LI (1988) Isolation and properties of minB, a complex genetic locus involved in correct placement of the division site in *Escherichia coli*. *Bacteriology* 170:2106-2112.

3. De Boer PAJ, Crossley RE, & Rothfield LI (1989) A division inhibitor and a topological specificity factor coded for by the minicell locus determine proper placement of the division septum in *E. coli*. *Cell* 56:641-649.

4. Pichoff S, Vollrath B, Touri C, & Bouche J (1995) Deletion analysis of gene minE which encodes the topological specificity factor of cell division in *Escherichia coli*. *Molecular Biology* 18:321-329.

5. al Ge (2000) Principles of Bacterial Pathogensis. *Academic Press*.

6. Ota KV*, et al.* (2009) Prevalence of and risk factors for quinolone-resistant *Neisseria gonorrhoeae* infection in Ontario. *Canadian Medical Association* 180:287-290.

7. Tapsall J (2009) Multidrug-resistant *Neisseria gonorrhoeae*. *Canadian Medical Association* 180:268-269.

8. Tapsall J (2001) Antimicrobial resistance in *Neisseria gonorrhoea*. *World Health Organization*

9. Kleckner N (2010) Mesoscale spatial patterning in the *E. coli* Min system: reaction-diffusion versus mechanical communication. *Proceedings of the National Academy of Science* 107:8053-8054.

10. Szeto J, Acharya S, Eng NF, & Dillon JR (2004) The N terminus of MinD contains determinants which affect its dynamic localization and enzymatic activity. *Bacteriology* 186:7175-7185.

11. Larkin MA*, et al.* (2007) ClustalW and clustalX version 2. *Bioinformatics* 23:2947-2948.

12. Waterhouse AM, Procter JB, Matrin DM, Clamp M, & Barton GJ (2009) Jalview Version 2 - a multiple sequence alignment editor and analysis workbench. *Bioinformatics* 25:1189-1191.

13. Cordell SC & Lowe J (2001) Crystal structure of the bacterial cell division regulator MinD. *Science* 492:160-165.

14. Hu Z, Mukherjee A, Pichoff S, & Lutkenhaus J (1999) The MinC component of the division site selection system in *E. coli* interacts with FtsZ and prevents polymerization. *Proceedings of the National Academy of Science* 96:14819-14824.

15. Hu Z & Lutkenhaus J (2000) Analysis of MinC reveals two independent domains invovled in interaction with MinD and FtsZ. *Bacteriology* 182:3965-3971.

16. Huang J, Cao C, & Lutkenhaus J (1996) Interaction between FtsZ and inhibitors of cell division. *Bacteriology* 178:5080-5085.

17. Pitchoff S & Lutkenhaus J (2002) Tethering the Z ring to the membrane through a conserved membrane targeting sequence in FtsA. *EMBO* 21:685-693.

18. Ward JE & Lutkenhaus J (1985) Overproduction of FtsZ induces minicell formation in *E. coli*. *Cell* 42:941-949.

19. Szeto J, Eng NF, Acharya S, Rigden MD, & Dillon JR (2005) A conserved polar region in the cell division site determinant MinD is required for responding to MinE-induced oscillation but not for localization within coiled arrays. *Research in Microbiology* 156:17-29.

20. Raskin DM & De Boer PAJ (1999) Rapid pole-to-pole oscillation of a protein required for directing division to the middle of *Escherichia coli*. *Proceedings of the National Academy of Science* 96:4971-4976.

21. Hu Z & Lutkenhaus J (2003) A conserved sequence at the C-terminus of MinD is required for binding to the membrane and targeting MinC to the septum. *Molecular Biology* 47:345-355.

22. Szeto TH, Rowland SL, Habrukowich CL, & King GF (2003) The MinD membrane targeting sequence is a transplantable lipid-binding helix. *Biological Chemistry* 278:40050-40056.

23. Zhou H & Lutkenhaus J (2003) Membrane binding by MinD involves insertion of hydrophobic residues within the C-terminal amphipathic helix into the bilayer. *Bacteriology* 185:4326-4335.

24. Zhou H & Lutkenhaus J (2005) MinC mutants deficint in MinD-and DicB-mediated cell division inhibition due to loss of interaction with MinD, DicD, or a septal component. *Bacteriology* 187:2846-2857.

25. Lackner LL, Raskin DM, & De Boer PAJ (2003) ATP-dependent interactions between *Escherichia coli* Min proteins and the phospholipid membrane in vitro. *Bacteriology* 185:735-749.

26. Raskin DM & De Boer PAJ (1999) MinDE-dependent pole-to-pole oscillation of division inhibitor MinC in *Escherichia coli*. *Bacteriology* 181:6419-6424.

27. Okuno T, Ogoh M, Tanina H, Funasaki N, & Kogure K (2009) Direct monitoring of interaction between *Escherichia coli* proteins, MinC and monomeric FtsZ, in solution. *Biological and Pharmaceutical Bulletin* 32:1473-1475.

28. Ma L, King GF, & Rothfield L (2004) Positioning of the MinE binding site on the MinD surface suggests a plausible mechanism for activation of the *Escherichia coli* MinD ATPase during division site selection. *Molecular Biology* 54:99-108.

29. Hu Z, Saez C, & Lutkenhaus J (2003) Recruitment of MinC, an inhibitor of Z-Ring formation, to the membrane in *Escherichia coli*: role of MinD and MinE. *Bacteriology* 185:196-203.

30. Hu Z & Lutkenhaus J (2001) Topological regulation of cell division in *E. coli*: spatiotemporal oscillation of MinD requires stimulation of its ATPase by MinE and phospholipid. *Molecular Cell* 7:1337-1343.

31. Ghasriani H*, et al.* (2010) Appropriation of the MinD protein-interaction motif by the dimeric interface of the bacterial cell division regulator MinE. *Proceedings of the National Academy of Science* 107:18416-18421.

32. Suefuji K, Valluzzi R, & Raychaudhuri D (2002) Dynamic assembly of MinD into filament bundles modulated by ATP, phospholipids, and MinE. *Proceedings of the National Academy of Science* 99:16776-16781.

33. Hayashi I, Oyama T, & Morikawa K (2001) Structural and functional studies of MinD ATPase: implications for the molecular recognition of the bacterial cell division apparatus. *EMBO* 20:1819-1828.

34. Sakai N*, et al.* (2001) The three-dimensional structure of septum site-determining protein MinD from *Pyrococcus horikoshii* OT3 in complex with Mg-ADP. *Structure Science* 9:817-826.

35. Wu W, Park K, Holyyoak T, & Lutkenhaus J (2011) Determination of the structure of the MinD–ATP complex reveals the orientation of MinD on the membrane and the relative location of the binding sites for MinE and MinC. *Molecular Microbiology* 79:1515-1528.

36. Zhou H & Lutkenhaus J (2004) The switch I and II regions of MinD are required for binding and activating MinC. *Bacteriology* 186:1546-1555.

37. Koonin EV (1993) A superfamily of ATPases with diverse functions containing either classical or deviant ATP-binding motif. *Molecular Biology* 229:1165-1174.

38. Zhou H*, et al.* (2005) Analysis of MinD mutations reveals residues required for MinE stimulation of the MinD ATPase and residues required for MinC interaction. *Bacteriology* 187:629-638.

39. Park K*, et al.* (2011) The Min oscillator uses MinD-dependent conformational changes in MinE to spatially regulate cytokinesis. *Cell* 146:396-407.

40. Shih Y, Le T, & Rothfield L (2003) Division site selection in *Escherichia coli* involves dynamic redistribution of Min proteins within coiled structures that extend between the two cell poles. *Proceedings of the National Academy of Science* 100:7865-7870.

41. Hu Z, Gogol EP, & Lutkenhaus J (2002) Dynamic assembly of MinD on phospholipid vesicles regulated by ATP and MinE. *Proceedings of the National Academy of Science* 99:6761-6766.

42. Fu X, Shih Y, Zhang Y, & Rothfield LI (2001) The MinE ring required for proper placement of the division site is a mobile structure that changes its cellular location during the *Escherichia coli* division cycle. *Proceedings of the National Academy of Science* 98:980-985.

43. Loose M, Fischer-Friedrich E, Ries J, Kruse K, & Schwille P (2008) Spatial regulators for bacterial cell division self-organize into surface waves *in vitro*. *Science* 320:789-792.

44. Loose M, Fischer-Friedrich E, Herold C, Kruse K, & Schwille P (2011) Min proteins patterns emerge from rapid rebinding and membrane interaction of MinE. *Nature Structural and Molecular Biology* 18:577-583.

45. Turing A (1952) The chemical basis of morphogenesis *Phiosophical Transations of the Royal Society of London* 327:37-72.

46. Kondo S & Miura T (2010) Reaction-diffusion model as a framework for understanding biological pattern formation. *Science* 329:1616-1620.

47. Mileykovskaya E*, et al.* (2003) Effects of phospholipid composition on MinD-membrane interactions *in vitro* and *in vivo*. *Biological Chemistry* 278:22193-22198.

48. Mazor S*, et al.* (2008) Mutual effects of MinD-membrane interaction: I. changes in the membrane properties induced by MinD binding. *Biochimica et Biophysica Acta* 1778:2496-2504.

49. Barak I, Muchova K, Wilkinson AJ, Toole PJ, & Pavlendova N (2008) Lipid spirals in Bacillus subtilis and their role in cell division. *Molecular Microbiology* 68:1315-1327.

50. Mileykovskaya E & Dowhan W (2005) Role of membrane lipids in bacterial division-site selection. *Current Opinion in Microbiology* 8:135-142.

51. Mazor S*, et al.* (2008) Mutual effects of MinD-membrane interaction: II. changes in the membrane properties induced by MinD binding. *Biochimica et Biophysica Acta* 1778:2505-2511.

52. Kruse K, Howard M, & Margolin W (2007) An experimentalist's guide to computational modelling of the Min system. *Molecular Microbiology* 63:1279-1284.

53. Dowhan W (2009) Molecular genetic approaches to defining lipid function. *Lipid Research*:S305-S310.

54. Ivanov V & Mizuuchi K (2010) Multiple modes of interconverting dynamic pattern formation by bacterial cell division proteins. *Proceedings of the National Academy of Science* 107:8071-8078.

55. Lopes S & Gameiro P (2010) Cardiolipin, a key component to mimic the *E. coli* bacterial membrane in model systems revealed by dynamic ligh scattering and steady-state fluorescence anisotropy. *Analytical and Bioanalytical Chemistry* 398:1357-1366.

56. Lewis TL & McElhaney RW (2009) The physicochemical properties of cardiolipin bilayers and cardiolipin-containing lipid membranes. *Biochimica et Biophysica Acta* 1788:2069-2079.

57. Guan J, Takamoto K, Almo SC, Reisler E, & Chance MR (2005) Structure and dynamics of the actin filament. *Biochemistry* 44:3166-3175.

58. Perkins DN, Pappin DJ, Creasy DM, & Cottrell JS (1999) Probability-based protein identification by searching sequence databases using mass spectrometry data. *Electrophoresis* 20:3551-3567.

59. Konermann L, Tong X, & Pan Y (2008) Protein structure and dynamics studied by mass spectrometry: H/D exchange, hydroxyl radical labeling, and related approaches. *Mass Spectrometry* 43:1021-1036.

60. Pan Y & Konermann L (2010) Membrane protein structural insights from chemical labeling and mass spectrometry. *Analyst* 135:1191-1200.

61. Engen JR (2009) Analysis of protein conformation and dynamics by hydrogen/deuterium exchange MS. *Analytical Chemistry* 81:7870-7875.

62. Garcia RA, Pantazatos D, & Villarreal FJ (2004) Hydrogen/deuterium exchange mass spectrometry for investigating protein-ligand interactions. *Assay and Drug Development Technologies* 2:81-91.

63. Xu G & Chance R (2007) Hydroxyl radical-mediated modification of proteins as probes for structural proteomics. *Chemical Reviews* 107:3514-3543.

64. Meltretter JaP, M. (2008) Application of mass spectrometry for the detection of glycation and oxidation products in milk proteins. *New York Academy of Science* 1126:134-140.

65. LLoyd RV, Hanna PM, & Mason RP (1997) The origin of the hydroxyl radical oxygen in the Fenton reaction. *Free Radical Biology and Medicine* 22:885-888.

66. Stadtman E (1993) Oxidation of free amino acids and amino acid residues in proteins by radiolysis and by metal-catalyzed reactions. *Annual Review of Biochemistry* 62:797-821.

67. Xu G & Chance M (2005) Radiolytic modification of sulfur-containing amino acid residues in model peptides: fundamental studies for protein footprinting. *Analytical Chemistry* 77:2437-2449.

68. Amici A, Levine RL, Tsai L, & Stadtman ER (1989) Conversion of amino acid residues in proteins and amino acid homopolymersto carbonyl derivatives by metal-catalyzed oxidation reactions. *Biological Chemistry* 264:3341-3346.

69. Barcelo D ed (2009) *Comperhensive Analytical Chemistry* (Wilson & Wilson's, Spain), Vol 52, pp 150-155.

70. Fox JE (2009) An introduction to MALDI. *Alta Bioscience*:91-94.

71. Stump MJ*, et al.* (2002) Matrix-assisted laser desorption mass spectrometry. *Applied Spectroscopy Reviews* 37:275-303.

72. Strupat K (2005) Molecular weight determination of peptides and proteins by ESI and MALDI. *Methods in Enzymology* 405:1-36.

73. Hunt SM & Sheil MM (1998) Comparison of electrospray ionisation mass spectromerty with matrix-assisted laser desorption ionisation mass spectrometry and the size exclusion chromatography for the characterization of polyester resins. *European Mass Spectrom* 4:475-486.

74. Hernandez P, Muller M, & Appel R (2006) Automated protein identification by tandom mass spectrometry: issues and startegies *Mass Spectrometry Reviews* 25:235-254.

75. Glish GL & Vachet RW (2003) The basics of mass spectrometry in the twentyfirst century. *Nature Reviews* 2:140-150.

76. Ramos D*, et al.* (2006) Conformation of the cell regulator MinE: evidencefor interactions between the topological specificity and anti-MinCD domains. *Biochemistry* 41:4593-4601.

77. Ausubel F*, et al.* (2001) *Molecular biology: protocols and clinical applications* (Jonh Wiley & Sons, Inc).

78. Ford KG, Whitmarsh AJ, & Hornby DP (1994) Overexpression and purification of eukaryotic transcription factors as glutathione-S-transferase fusions in *E. coli*. *Molecular Biology* 30:185-197.

79. Wiechelman K, DBraun R, & Fitzpatrick J (1988) Investigation of the bicinchoninic acid protein assay: Identification of the groups responsible for color formation. *analytical biochemistry* 175:231-237.

80. Smith PK*, et al.* (1985) Measurement of protein using bicinchoninic acid. *Analytical Biochemistry* 150:76-85.

81. De Boer P, Crossley R, Hand A, & Rothfield L (1991) The MinD protein is a membrane ATPase required for the correct placement of the Escherichia coli division site. *European Molecular Biology Organization* 10:4371-4380.

82. Zhu Y*, et al.* (2009) Elucidating in vivo structural dynamics in integral membrane protein by hydroxyl radical footprinting. *Molecular and Cellular Proteomics* 8:1999-2010.

83. King G & al e (1999) The dimerization and topological specificity functions of MinE reside in structurally autonomous C-terminal domain. *Molecular Microbiology* 31:1161-1169.

84. Eng NF, Szeto J, Acharya S, Tessier D, & Dillion JA (2006) The C-terminus of MinE from *Neisseria gonorrhoeae* acts as a topological specificity factor by modulating MinD activity in bacterial cell division. *Review in Microbiology* 157:333-344.

85. Hart CT (2008) Functional and structural studies of the anti-MinCD domain of MinE. Msc thesis (University of Ottawa).

86. Kabaso D*, et al.* (2011) Exploring the binding dynamics of bar proteins. *Cellular and Molecular Biology* 16:398-411.

87. Abedin A (2011) Structural and functional studies of the bacterial cell division protein MinD: implications of the C-terminus. MSc thesis (University of Ottawa).

88. Plowman JE*, et al.* (2003) The effect of oxidation or alkylation on the separation of wool keratin proteins by two-dimensional gel electrophoresis. *Proteomics* 6:942-950.

89. Sambrook J, Fritsch E, & Maniatis T (1989) *Molecular cloning: a laboratory manual* (Cold Spring Harbor Laboratory N.Y).

90. Marangoni AG (2003) *Enzyme kinetics: a modern approach* (John Wiley & Sons, Inc. , New Jersey).

91. Park K, Wu W, Lovell S, & Lutkenhuas J (2012) Mechanism of the asymmetric activation of the MinD ATPase by MinE. *Molecular Microbiology* 85:271-281.

92. Silberg JJ & Vickery LE (2000) Kinetic characterization of the ATPase cycle of the molecular chaperone Hsc66 from *Escherichia coli*. *Biological Chemistry* 275:7779-7786.

93. Gasmi-Seabrook GMC*, et al.* (2010) Real-time NMR study of guanine nucleotide exchange and activation of RhoA by PDZ-RhoGEF. *Biological Chemistry* 285:5137-5145.

94. Crooks GE, Hon G, Chandonia JM, & Brenner SE (2004) Weblogo: a sequence logo generator. *Genome Research* 14:1188-1190.

95. Schneider TD & Stephens RM (1990) Sequence logos: a new way to display consensus sequences. *Nucleic Acids Research* 18:6097-6100.

96. Matsumoto K, Kusaka J, Nishibori A, & Hara H (2006) Lipid domains in bacterial membranes. *Molecular Microbiology* 61:1110-1117.

97. Zerrouk Z, Alexandre S, Lafontaine C, Norris V, & Valleton J (2008) Inner membrane lipids of *Escherichia coli* form domains. *Biointerfaces* 63:306-310.

98. Renner LD & Weibel DB (2011) Cardiolipin microdomains localize to negatively curved regions of *Escherichia coli* membranes. *Proceedings of the National Academy of Science* 108:6264-6269.

Appendix

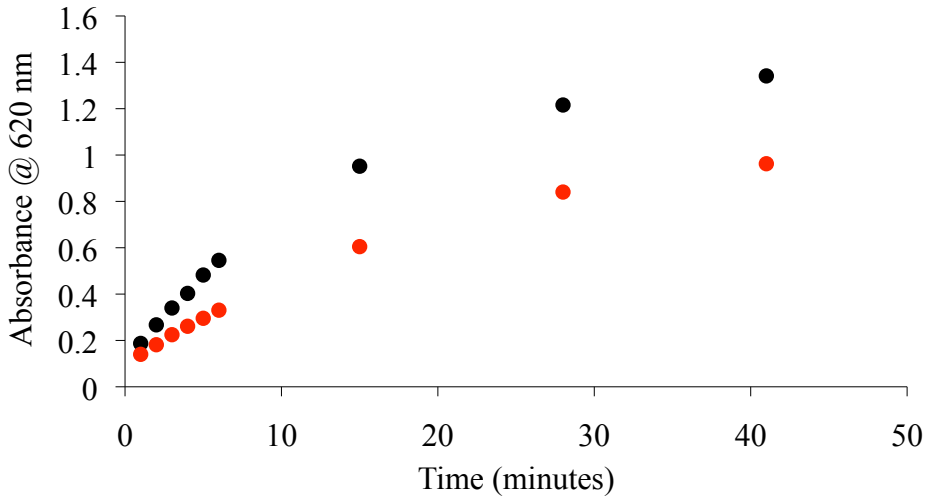

A.1: Test of sample dilution on kinetic profiles for MinE-stimulated MinD ATPase activity with DOPG. *Assay samples (black, as shown in Figure 3.8) were diluted by adding an equal volume of size exclusion buffer to each sample after boiling and centrifugation, prior to addition to malachite green reagent (red).*

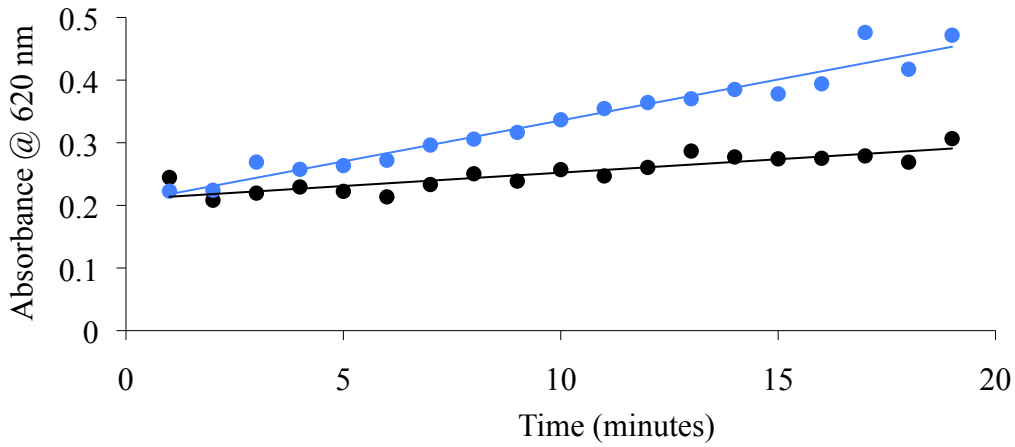

A.2: MinD ATPase activity under lipid tubule-promoting conditions*. 6 μM MinD, 80 μg/ml E. coli phospholipids and 0 (black) and 0.1 (blue)) μM MinE. In contrast with previous studies (41), no lag phase is observed.*